The dynamic response of oceanic hydrate deposits to ocean temperature change

Matthew T. Reagan and George J. Moridis

Earth Sciences Division

Lawrence Berkeley National Laboratory

1 Cyclotron Rd.

Berkeley, CA 94720, USA

Abstract

Vast quantities of methane are trapped in oceanic hydrate deposits. Because methane is a powerful greenhouse gas (about 26 times more effective than CO_2), there is considerable concern that a rise in the temperature of the oceans will induce dissociation of oceanic hydrate accumulations, potentially releasing large amounts of carbon into the atmosphere. Such a release could have dramatic climatic consequences because it could amplify atmospheric and oceanic warming and possibly accelerate dissociation of the remaining hydrates. This study assesses the stability of three types of hydrates—I) deep-ocean deposits, II) shallow, warm deposits, and III) shallow, cold deposits—and simulates the dynamic behavior of these deposits under the influence of moderate ocean temperature increases. The results indicate that deep-ocean hydrates are stable under the influence of moderate increases in ocean temperature; however, shallow deposits can be very unstable and release significant quantities of methane under the influence of as little as 1 ^{o}C of seafloor temperature increase. Less permeable sediments, or burial underneath layers of hydrate-free sediment, affect both the rate of hydrate dissociation and methane transport to the seafloor, but may not prevent methane release. Higher-saturation deposits can produce larger methane fluxes with the thermodynamics of hydrate dissociation retarding the rate of recession of the upper hydrate interface. These results suggest possible worst-case scenarios for climate-change-induced methane release, and point toward the need for detailed assessment of the hydrate hazard and the coupling of hydrate-derived methane to regional and global ecosystems.

Index Terms: 1605, 1635, 1807, 1847, Keywords: gas hydrates, climate change

Introduction

Gas hydrates

Gas hydrates are solid crystalline compounds in which gas molecules are lodged within the lattices of water clathrate crystals (Sloan, 1998). Natural gas hydrate deposits occur in two distinctly different geologic settings where the necessary low temperatures and high pressures exist for their formation and stability: in the permafrost and in deep ocean sediments. A review of the literature on the subject indicates that (a) estimates of in situ methane hydrate reserves are enormous, ranging between 10^{15} m^3 STP (Milkov, 2004) to as high as $7.6x10^{18}$ m^3 STP (Dobrynin et al., 1981). The dissociation reaction of methane hydrate can be described by the equation:

$$CH_4 \bullet N_H\, H_2O \rightarrow CH_4 + N_H\, H_2O \qquad (1)$$

where N_H is the hydration number that may vary between 5.75 (for complete hydration) and 7.21, with a typical range of 5.81-6.10 and an average value of $N_H = 5.99$ (Circone et al, 2005). The three main methods of hydrate dissociation are: (1) depressurization, in which the pressure is lowered below the hydration pressure P_H at the prevailing temperature, (2) thermal stimulation, in which the temperature is raised above the hydration temperature T_H at the prevailing pressure, and (3) the use of inhibitors (such as salts and alcohols), which causes a shift in the P_H-T_H equilibrium through competition with the hydrate for guest and host molecules (Sloan, 1998).

In oceanic deposits, the range of depth over which hydrates remain stable depends on the pressure P (imposed by the water depth) and temperature T. Figure 1 (Moridis and

Kowalsky, 2005) shows the phase diagram as defined by the P_H - T_H equilibrium of methane hydrate (the dominant gas in natural hydrate deposits). A pressure decrease due to lowering of the sea level, or an increase in the temperature of the ocean water in contact with the seabed, could induce hydrate dissociation and lead to the release of gas. The released CH_4 could be transferred to the exchangeable carbon reservoir by ebullition or diffusion into the water column, advection by the water current, chemical and biochemical oxidation reactions in the water column, and finally by ebullition into the atmosphere if the rate of CH_4 release were to exceed the rate of oxidation (Kennett et al., 2000).

Assessment of the hydrate resource

The methane trapped as hydrate in ocean sediments originates from biological sources through decay of organic matter accumulated at the seafloor, or through upward migration of thermogenic methane from deeper deposits. The slow, constant process of "organic rain" provides a source for methanogenesis, and the resulting methane moves into benthic sediments via burial and compaction of sediments and fluid flow within sediments (Gornitz and Fung, 1994; Xu and Ruppel, 1999; Buffett and Archer, 2004). This methane may combine with seawater to form methane hydrate wherever temperature and pressure conditions are suitable. Hydrates found in the deep ocean (> 1000 m) have been the primary focus of most previous investigations. Such hydrates are clearly stable because of pressures well above, and temperatures below, the hydrate Lw+H+V phase boundary (see Figure 1). Stable hydrate may also exist closer to the surface--experimental phase diagrams and ocean drilling evidence indicate a gas hydrate stability zone (GHSZ)

below 300 m water depth on the continental shelf in cold arctic waters and below 440 m depth in the warmer Gulf of Mexico (Milkov and Sassen, 2001), and extending deep into the sediment column.

Many investigators have attempted to assess the total amount of methane hydrate currently residing in the deep ocean and along continental margins. These estimates began with the work of Makagon (1974), and lead, subsequently, to an initial "consensus value" of 10,000 Gt through work by various investigators (Gornitz and Fung, 1994; Holbrook et al., 1996; Kvenvolden, 1999; Borowski, 2004), who used thermodynamic modeling to define regions of possible hydrate stability and data from sediment cores and seismic profiles to characterize the sediment environment. In a detailed assessment of existing estimates, Milkov (2004) proposed a total of 500-2,500 Gt of methane carbon (1-5 x 10^{15} m^3 STP), while acknowledging earlier estimates indicating larger quantities. This skepticism was supported by geophysical data indicating heterogeneities in temperature and salinity in the Gulf of Mexico (Ruppel et al., 2005) that could impede gas hydrate formation and stability. Recently, two global studies that account for the coupled contribution of organic matter decomposition and mass transport have produced drastically different results. The first (Klauda and Sandler, 2005) used an equilibrium thermodynamic model coupled to a mass-transfer model for hydrate formation to provide an upper estimate of 74,400 Gt of methane in hydrate form (27,300 Gt along continental margins). The second (Buffett and Archer, 2004) simulated the formation of steady-state methane hydrates from organic decomposition and used both compaction and advection in a 1-D methanogenesis/hydrate formation model to reach an estimate of 3,000 Gt of

methane in hydrates and 2,000 Gt of gaseous methane existing in a stable state under current climate conditions.

The hydrate stability zone may extend upward to 300 m - 400 m water depths (Moridis and Kowalsky, 2005), and such shallow deposits are more prone to destabilization due to their proximity to the Lw+H+V phase boundary and the shorter time needed for temperature changes to propagate through the hydrate-bearing sediments (HBS). Shallow deposits may also be at greater risk for destabilization than estimated by broad global surveys. The Gulf of Mexico, in particular, may contain up to 500 Gt of carbon stored as methane hydrate in its sediments (Collett and Kuuskraa, 1998). Other studies give lower estimates of hydrate extent, but also postulate that a temperature change of 4^{o}C could result in 30% thinning of the GHSZ, possibly destabilizing 2 Gt of hydrate (Milkov and Sassen, 2003). Hundreds of Gt of methane are expected to exist within Arctic Ocean sediments (Archer, 2007), and no conclusive studies have assessed its distribution, form, or possible fate.

Hydrate instability due to climate change

An increase in the temperature of the ocean water at the seafloor could induce hydrate dissociation and lead to gas release. Such a release could have potentially dramatic climatic consequences because it could lead to a cascading sequence of events, involving amplified atmospheric and oceanic warming and accelerated dissociation of the remaining hydrates. Recent deep ocean surveys have found pockmarks and other structures that indicate large fluid releases at the seafloor in the past (Hovland et al.,

2005) and hydrate dissociation and gas release is either a possible cause or consequence of submarine slope failure and landslides (Dickens et al., 1995). Other computational studies also show the potential for hydrate instability and methane release under warming conditions (Milkov and Sassen, 2003; Hornbach et al., 2004; Buffett and Archer, 2004). Coupling of a simple global clathrate reservoir to a time-dependent ocean carbon cycle model (Archer and Buffett, 2005) showed a significant contribution to climate change on millennial timescales. Most recently, dynamic simulations of dissociation in response to temperature changes (Reagan and Moridis, 2007) indicated that shallow systems can release significant quantities of methane on decadal timescales when subjected to as little as 1 ^{o}C of warming applied to the top of the sediment column. In contrast, simulations of the behavior of deep, cold, steady-state hydrates subjected to up to 10 ^{o}C of warming (Xu and Lowell, 2001; Reagan and Moridis, 2007) do not indicate widespread instability or methane release due to changes in the extent of the GHSZ alone. Under these conditions, temperature changes modify the geothermal gradient and change the distribution and saturation of hydrates within the deposit.

The "Clathrate Gun" Hypothesis (Kennett et al., 2002), postulated that marine hydrate accumulations undergo repeated cycles of reloading and discharge, with hydrates accumulating during cold glacial intervals and dissociating when triggered by pulses of warmer water impinging on the continental slopes. In the past, increases in water temperatures near the seafloor caused by climatic changes may have caused dissociation of accumulated hydrate deposits. This could have resulted in the release of large quantities of methane into the ocean, and into the atmosphere via ebullation, advection,

and gas exchange, with a methane spike reflected in sediment cores and paleoclimatic data. This mechanism, still considered controversial, could have greatly amplified and accelerated global warming episodes, leading to temperature increases of 5-10 ^{o}C in as few as 30 years, further increasing atmospheric and oceanic warming, and accelerating dissociation of the remaining hydrates. Such hydrate dissociation has been proposed as a significant mechanism to explain the rapid and significant climate changes in the late Quaternary period (Kennett et al., 2000), and to explain the severity of natural climate cycles. Dramatic increases in methane concentrations in polar ice (Brook et al., 1996) and in the atmosphere (Severinghaus et al., 1998) during the Quaternary period, δ^{13}C isotopic excursions in benthic foraminifera (Kennett et al., 2000), evidence of widespread benthic extinctions (Kennett and Stott, 1991), and evidence of major methane release from the ocean floor through sediment disruption during that period (Kvenvolden, 1988; Rothwell et al., 1998) appear to support this hypothesis and underline concerns about the possibility of hydrate-mediate climate forcing. Isotopic analysis of Marinoan glacial marine deposits (Kennedy et al., 2008) also suggest that rapid warming and deglaciation at the end of the Cryogenian "snowball Earth" period may have been triggered and/or supported by clathrate-derived methane. Kinetic modeling of carbon reservoir discharge compared with data from ice cores also suggests that observed methane concentration changes in the late Quaternary are consistent with the magnitude and rapidity of proposed shallow clathrate decomposition (O'Hara, 2008).

The Clathrate Gun hypothesis has been challenged by different interpretations of the paleoclimatic data, estimations of actual hydrate extent, and simulations modeling

hydrate stability. Kvenvolden (1999) suggests that methane from dissociating hydrates may never reach the atmosphere, converting to carbon dioxide in the water column or being sequestered in the biosphere. Once exposed to the environment of the open ocean, methane is subject to conventional oxidation (Valentine et al., 2001), although it may be transported through the upper region of the water column where atmospheric ventilation times are short compared to oxidation rates (Brewer et al., 2002). Isotopic studies of air trapped in ice cores (Sowers, 2006) question the source of the atmospheric methane during these rapid temperature excursions, and Nisbet (2002), while suggesting methane as a factor in moderating glaciation, proposed that the methane spikes may follow, not lead, climate change. Simulations of deep ocean hydrates (Xu and Ruppel, 1999; Xu and Lowell, 2001; Reagan and Moridis, 2007) show that deep (>1000m) hydrates may be relatively insensitive to ocean temperature shifts on short time scales. Other studies, relying on simplified thermodynamic and transport models of hydrate-bearing sediments, have argued that hydrate stability may be enhanced by the thermal properties of the overlying sediment column, within which the hydrates are sparsely distributed (Archer, 2007). That the clathrate gun hypothesis has been criticized, but no conclusive evidence has been put forth to discount the possible importance of hydrate-derived methane in climate cycles, suggests that a careful assessment of the stability of existing oceanic clathrates is required.

The process of dissociation and release is illustrated schematically in Figure 2. An increase in ocean water temperature at the seafloor, from temperature profile (1) to profile (2), lowers the top of the GHSZ (A) and raises the bottom of the GHSZ (B) as the

temperature profile intersects a reduced region of the hydrate stability curve (the excluded area shaded in green). In this illustration, any hydrate existing in the sediments at depths near (B) is destabilized and may dissociate. The GHSZ may extend above the seafloor (as shown), or the top of the GHSZ may lie at or below the seafloor. The process of hydrate dissociation is regulated by multiple factors, including flow of heat from the surroundings, fluid flow induced by hydrate dissociation, the thermal properties of the sediments (regulating the propagation of temperature changes into the sediment column), and the enthalpy of dissociation of the hydrates themselves. In the following computational study, we analyze the coupled thermodynamic, hydrologic, and transport processes that occur in oceanic hydrate deposits subjected to thermal loading.

Methods

Simulation tools

The TOUGH+HYDRATE code (Moridis et al., 2008) used in this study describes multiphase flow and transport in hydrate-bearing geologic media. It includes coupled mass and energy transport within porous and/or fractured media, and also describes the full phase behavior of water, methane, solid hydrate, ice, and inhibitor species (Moridis, 2003). The TOUGH+HYDRATE code has been used to (a) design the first field test of gas production from hydrate deposits in the Mallik area, Mackenzie Delta, Northwest Territories, Canada (Moridis, 2002; 2004; Moridis et al., 2004; Moridis et al., 2005a), (b) to analyze the results of the field study and determine the values of important parameters (Moridis et al., 2005a), (c) to evaluate the gas production potential of hydrates from both

permafrost and ocean accumulations (Moridis et al., 2007; Moridis and Kowalsky, 2005; Moridis and Sloan, 2007; Moridis and Reagan, 2007a, 2007b), and (d) to investigate the effects of hydrate dissociation on the geomechanical stability of hydrate-bearing sediments (Moridis and Kowalsky, 2007; Rutqvist and Moridis, 2007). This code, also validated in laboratory experiments (Moridis et al., 2005a; Tang et al., 2007), was recently used in preliminary studies of hydrate dissociation in oceanic sediments (Reagan and Moridis, 2007). This work is a continuation and expansion of that research.

Setup of 1-D system

We simulate three types of hydrate accumulations, each representing disperse, low-saturation deposits with an initial hydrate saturation, S_{H0}, of 0.03 (Moridis and Sloan, 2007) reflecting the high end of the estimated global average saturation (Archer, 2007) for stratigraphic deposits.

Case I. The first case involves deep, cold hydrate deposits at a depth of 1000 m, with an initial seafloor temperature of T_0 = 4 ˚C and a geothermal gradient of 3.5 ˚C/100 m (Xu and Lowell, 2001). These conditions indicate stable hydrate, with the top of the GHSZ well above the seafloor.

Case II. The second case involves a shallow, warmer hydrate deposit at 570 m depth, T_0 = 6 ˚C, and a geothermal gradient of 2.8 ˚C/100m. This case is representative of Gulf of Mexico deposits (Milkov and Sassen, 2001), with the top of the GHSZ near the seafloor.

Case III. The third case describes shallow, cold hydrate deposits at 320 m depth, T_0 = 0.4 ˚C, geothermal gradient of 3 ^{o}C/100m, representative of conditions on the arctic continental shelf, with the top of the GHSZ located at the seafloor.

The representation of each case in this study involves a vertical, 1-D domain describing the sediment column from the seafloor. The initial condition includes a hydrostatic pressure distribution, a constant geothermal gradient, and a uniform hydrate saturation in the sediment column from the seafloor to the bottom of the GHSZ. These deposits are assumed to be at steady state before any temperature changes occur, and are not connected to active seeps or methane sources. Physical parameters for the sediments are listed in Table 1. The intrinsic permeability, $k = 10^{-15}$ m^2 (1.0 mD), is within the reported range of oceanic sediments (Ginsberg and Soloviev, 1998; Spinelli et al., 2004) and represents the more common stratigraphic deposits (Milkov, 2004; Moridis and Sloan, 2007), in contrast to the less common, more permeable, and often more saturated structural deposits near sites of active methane seepage and/or venting. The porosity ϕ = 0.3 is typical for unconsolidated marine sediments near the mudline (Ginsberg and Soloviev, 1998).

For the dynamic simulations, constant pressure (corresponding to a constant ocean water depth and salinity) is maintained at the top of the sediment column, while the temperature at the top boundary (corresponding to the water at the ocean floor), is varied. The top of the sediment column is an open boundary, allowing heat and mass transfer

between the sediment and the ocean. The sediment column is modeled to a depth of 360 m below the seafloor, well beyond the reach of temperature propagation over the simulated period. The entire column is equilibrated to initial steady-state conditions to ensure stable temperature and pressure gradients and to establish hydrate distributions, saturations, and aqueous methane concentrations that correspond to the conditions at the selected depth and temperature.

Results from recent simulations coupling ocean circulation, atmospheric circulation, and atmospheric chemistry (Meehl et al., 2007) suggest that, under current climate conditions and a 1%/yr increase in atmospheric CO_2 concentration, the temperature at the seafloor would rise by 1 ˚C or more over the next 100 yr, and possibly by another 3 ^{o}C in the following century. The actual degree of warming and the time-temperature profiles vary greatly with location and model parameters (for example, the IPCC A1B scenario). Consequently, we restrict our representation of ocean warming to simple linear temperature increases of ΔT = 1, 3, and 5 ˚C over a 100 yr period to describe the evolution of ocean temperature at the seafloor. These linear functions are applied at the upper boundary of the 1-D domain. We record methane fluxes and fluid flow velocities at the seafloor, as well as the pressure, temperature, and phase saturation profiles at regular intervals. These cases, although rough schematics of the wide range of possible hydrate depths, distributions, and saturations, allow a systematic examination of the many coupled processes that drive and regulate possible hydrate dissociation.

Results

Temperature and saturation profiles

Case I: Deep, cold hydrate deposits. Figure 3 presents profiles of the 1-D distributions of hydrate saturation (S_H), gas saturation (S_G), and temperature (T) for Case I, undergoing a ΔT = 3 ^{o}C/100 yr temperature increase at the seafloor, at t = 0 yr (Figure 3a, initial condition) and t = 100 yr (Figure 3b1). Even after up to 3^{o}C of warming, the top of the GHSZ remains above the seafloor, and only solid hydrate is seen within the top 250 m of the sediment column. This confirms the relative insensitivity of deep hydrate systems (at high pressures) to moderate temperature changes at short time scales. These results agree with previous investigations of deep oceanic hydrates (Xu and Lowell, 2001). The pressure distribution within the sediment column (Figure 3b2) after t = 100 yr shows no driving force for fluid flow, with the pressure distribution essentially unchanged from the initial hydrostatic distribution. Because methane release at the seafloor is essentially nonexistent, no injection of carbon into the ocean is expected on short timescales from such deep deposits from changes in the temperature profile alone.

Case II: Warm, shallow hydrate deposits. Profiles of S_H, S_G, and temperature for Case II undergoing a ΔT = 3 ^{o}C/100yr temperature increase at the seafloor, reported previously in Reagan and Moridis (2007), are presented in Figure 4a through 4c. The initial S_H and S_G (t = 0 yr) is shown in Figure 4a. As the temperature increase propagates downward, the profiles clearly show a much stronger, more rapid, and more dramatic response to changes in seafloor temperature. At t = 10 yr, Figure 4b provides a snapshot of the point at which the released gas first reaches the top of the sediment column, with a saturation

S_G = 0.064. Free gas, near the level of irreducible gas saturation, is also present throughout the deposit (S_G=0.01) at t = 10 yr, as dissociation proceeds quickly throughout the hydrate-bearing layer (HBL). The hydrate deposit for this case is thin, due to the narrow region of hydrate stability under Case II conditions, and at t = 100 yr all of the hydrate has dissociated (Figure 4c). A region of mobile gas ($S_G \leq 0.075$) occupies the previously hydrate-bearing sediments, rising through the sediment column and escaping at the seafloor.

Case III: Cold, shallow hydrate deposits. Profiles of T, S_H, and S_G for Case III undergoing a ΔT = 3 ^{o}C/100yr temperature increase at the seafloor are shown in Figures 5a through 5c. This system is shallow (depth of 320 m) but cold (T_0 = 0.4 ^{o}C), and the initial thickness of hydrate-bearing layer is considerably greater than in Case II (Figure 5a). In Figure 5b, at t = 10 yr, $\Delta T_{seafloor}$ = +0.3 ^{o}C, and the temperature disturbance has propagated 8-10 m into the sediment column. Rather than dissociation occurring throughout the deposit, as seen in Case II, a dissociation front with a thickness of approximately 6 m has formed and the top of the hydrate-bearing layer has receded to z = -5 m below the top of the sediment column. A plume of gaseous methane (S_G = 0.11) has formed between the dissociation front and the seafloor. The endothermic nature of the hydrate dissociation reaction results in a self-sharpening dissociation front as heat flowing downward from the warming ocean (along the inverted geothermal gradient) is absorbed by the topmost, dissociating layer of hydrate. In Figure 5c (t = 100 yr), the front has reached z = -65 with little noticeable disturbance in the temperature gradient below the zone of dissociation. A large zone of free gas (S_G = 0.11) fills the region voided by

the dissociating hydrate. At t = 100 yr, over 30% of the hydrate deposit remains, and the inverted geothermal gradient, still far from a new equilibrium, indicates that the process can be expected to continue at similar dissociation rates until the bottom of the hydrate-bearing layer is reached and the deposit is exhausted.

Release rates

Fluxes of methane, as measured at the open boundary at the top of the sediment column, are shown in Figure 6. The combined flux of methane in both the gas and aqueous phases for all three simulated linear temperature variations— $\Delta T_{seafloor}$ = 1, 3, and 5 ^{o}C/100 yr—is plotted vs. time for Case II and Case III and 570 m cases (seafloor fluxes for Case I are many orders of magnitude smaller, i.e. effectively nonexistent on this scale, and are not shown). Most notable is the near-order-of-magnitude difference between the instantaneous methane fluxes in the two cases, despite identical initial hydrate saturations and parallel temperature change scenarios.

Case II: Warm, shallow hydrate deposits. For Case II, as previously reported (Reagan and Moridis, 2007) the flux exhibits an initial peak, describing the transport of methane dissolved in the aqueous phase, followed by a second surge of methane, primarily in the gaseous phase. This lag between the beginning of dissociation (in which the expansion of gas formed during the initial dissociation drives methane-saturated fluids away from the dissociation zone and through the sediment column) and the arrival of mobile, buoyant gaseous methane at the seafloor is also reflected in the gap seen in Figure 4a between the top of the sediment column and the region with a significant S_G. The magnitude of ΔT

(and consequently, the rate of temperature increase) affects the rate of dissociation, as evidenced by both 1) lower instantaneous methane flux under more gradual change, and 2) a delay in the time of peak aqueous methane flux and the arrival of gaseous methane at the seafloor. Seafloor fluxes range from Q_{CH4} = 0.049 to 0.062 m^3 CH_4/yr at standard temperature and pressure (m^3/yr STP) per m^2 of seafloor, equivalent to Q_{CH4} = 2.2 - 2.8 mol CH_4/yr per m^2. Aqueous flow velocities at the top of the sediment column peak at 4.3 to 7.6 cm/yr.

Case III: Cold, shallow hydrate deposits. For the case representing the arctic continental shelf at 320 m and T_0 = 0.4 ^oC initial temperature, the arrival of significant methane flux at the seafloor is delayed for all cases compared to Case II. This is a consequence of several coupled effects. Although the top of the hydrate deposit is initially located at the top of the GHSZ for both Case II and Case III, and both cases are subjected to the same temperature perturbation, the colder hydrate deposit in Case III requires additional heat to induce dissociation. For this case, released methane in both the aqueous and gas phases arrives at the seafloor at roughly the same time, quickly reaches peak flux, and then maintains significant (and near-constant) fluxes throughout the 100 yr simulation timeframe. For each temperature, the peak instantaneous methane flux, Q_{CH4}, is up to 5 times greater than seen in Case II (Figure 6). Peak Q_{CH4} ranges from 0.18 m^3/yr STP (8 mol/yr) to nearly 0.3 m^3/yr STP (13 mol/yr) per m^2 of seafloor. These fluxes are similar in magnitude to methane fluxes observed at cold vent sites on Hydrate Ridge (Luff et al., 2005). They also exceed the integrated anaerobic methane oxidation rates computed for benthic sediments in the Hydrate Ridge region (Luff et al., 2005), an environment that is

both warmer and (presumably) more biologically active than the arctic continental shelf. These fluxes also approach the rates of methane consumption estimated for established chemosynthetic communities near active methane vent sites (Sassen et al., 1999; Boetius and Suess, 2004), therefore any assumed mitigation effect through benthic biochemistry represents a best-case scenario. Note that these simulations do not include benthic chemistry nor calculate the response of existing seafloor ecosystems to surges in methane flux.

Cumulative release

Cumulative fluxes, V_{CH4}, at the seafloor, shown in Figure 7, exhibit a factor of 5 difference in the total methane released into the environment over the 100 yr simulation period. For $\Delta T = 5\ ^{o}C$, approximately 23 m^3 STP (1020 mol) of gaseous and dissolved methane escapes, per m^2 of seafloor for Case III, while for $\Delta T = 1\ ^{o}C$ change, $V_{CH4} = 14\ m^3$ (620 mol). Case II, in contrast discharges $V_{CH4} = 3.4$ to 4.9 m^3 (150 to 220 mol) per m^2. Note that, in each of these cases, additional methane gas remains in the sediment column at $t = 100$ yr (and in Case III, solid methane hydrate remains as well), therefore the total possible release over long times is expected to be larger. Estimating temperature change scenarios past 100 yr, however, could be regarded as highly speculative, and therefore these simulations are restricted to 100 years. For any foreseeable temperature-change scenario, the 30% of the hydrate in Case III that remains at the end of the simulation time is unlikely to remain undissociated, and the released gas is unlikely to remain entirely entrained within the sediments.

Effect of sediment permeability

As discussed previously, the permeability of ocean sediments varies greatly—by up to seven orders of magnitude—depending on the porosity and sediment type (Spinelli et al., 2004). A common baseline assumption for unconsolidated marine sediments at the seafloor is a permeability of $k_0 = 10^{-15}$ m^2 (1.0 mD) and a porosity of $\phi = 0.3$ (Ginsberg and Soloviev, 1998), and this has been used as the reference, or base case in this study. However, the two regions examined here, the Gulf of Mexico and Arctic Ocean, are primarily underlain by terrigenous sediments, for which experimental and in-situ measurements have shown to have a range of permeabilities from $k = 10^{-12}$ to $k = 10^{-18}$ m^2 (1000 mD to 0.001 mD), with a large distribution of samples between $k = 10^{-13}$ and $k = 10^{-17}$ m^2 (100 mD to 0.01 mD) (Spinelli et al., 2004). To assess the sensitivity of hydrate dissociation and methane release to sediment permeability, the scenario of $\Delta T = 3$ ºC/100 yr temperature increase was simulated for systems with k ranging from 10^{-14} to 10^{-17} m^2, representing a likely range of sediment permeabilities, and additionally at $k = 10^{-13}$ m^2, representing a more permeable, sandy formation. The initial conditions for each system were re-equilibrated to steady state for each permeability, with all other properties held constant. Profiles of S_H and S_G were generated for the extreme cases 10^{-13} and 10^{-17} m^2 (100 mD and 0.01 mD), while the methane flux at the seafloor was assessed for all permeabilities.

Figure 8 shows the evolution of S_H and S_G over time and the effect of sediment permeability for Case II. Increased permeability, to $k = 10^{-13}$ m^2, results in no change in the position of the hydrate dissociation interface at $t = 10$ yr (Figure 8a) compared to the

base case, k_0, but there is a significant decrease in S_G in the region between the dissociation interface and the seafloor, indicating an increase in the amount of the released gas exiting the top of the sediment column for a given degree of hydrate dissociation. In contrast, a reduction in permeability to $k = 10^{-17}$ m^2 suppresses hydrate dissociation considerably, with only the topmost 1 m of hydrate having dissociated at 10 yr. By 100 yr (Figure 8b), the hydrate deposit is completely dissociated for all permeabilities. Note that the high-k sediments entrain considerably less gas at lower saturations than the base case, and conversely, the low-k case entrains more gas at higher saturations, with S_G reaching 0.075 to 0.08. Profiles of P vs. z (Figure 8c) reveal significant localized increases of $\Delta P = +0.7$ bar above the base case for a system with $k = 10^{-17}$ m^2. At the T,P conditions for Case II at $t = 10$ yr ($T_{seafloor} = 6.3$ °C, $P_{seafloor} = 57$ bar), this ΔP is sufficient to raise the top of the GHSZ and retard hydrate dissociation.

A comparison of instantaneous release rates for Case II over all four permeabilities (Figure 9) shows the variation in methane flux at the seafloor vs. sediment permeability. Methane flux at the seafloor transported via the aqueous phase, Q_{Aq}, is represented by solid lines, while methane flux in the gas phase, Q_G, is represented by dotted lines ($Q_{CH4} = Q_{Aq} + Q_G$). For $k = 10^{-14}$ m^2, the system exhibits no significant increase in Q_{Aq} compared to the base Case II ($k_0 = 10^{-15}$ m^2) up to $t = 11$ yr, followed by a dramatic change in both the time of arrival of gas ($\Delta t = -20$ yr) and the magnitude of Q_G, which peaks at $Q_G = 0.28$ m^3/yr STP, or 12.5 mol/yr per m^2 of seafloor. This is a six-fold increase in the rate of release over the base case, but is followed by a significant decline in gas release after $t = 40$ yr, reflecting the rapid depletion of the deposit. For the most

permeable case ($k = 10^{-13}$ m^2), 24 yr sooner than in the base case, with a sixteen-fold increase in methane flux (0.8 m^3/yr STP or 35.6 mol/yr per m^2 of seafloor) and rapid decline by $t = 24$ yr reflecting depletion of the deposit. Reduced permeability, $k = 10^{-17}$ m^2, however, results in both a decrease in Q_{Aq} and no gas flux at the seafloor over the 100 yr simulation period. As seen in Figure 8b, the gas phase remains entrained in the sediment column, with methane escape occurring via transport in the aqueous phase at rates not exceeding $Q_{Aq} = 0.016$ m^3/yr STP (0.71 mol/yr) per m^2 of seafloor—a significant decrease in comparison to all other simulated permeabilities.

For Case III, the effect of permeability on the evolution of the hydrate system is similar. Figure 10 shows profiles of S_H and S_G for all three permeabilities. A higher permeability ($k = 10^{-13}$ m^2) system dissociates only slightly more rapidly than the base case, k_0, up to $t = 10$ yr (Figure 10a), with lower S_G in the sediment column. Decreased permeability ($k = 10^{-17}$ m^2), as in Case II, produces slower dissociation, regulated by the stabilizing effects of a localized 0.6 bar increase in P over the base case, along with greater S_G within the sediment column. At $t = 100$ yr (Figure 10b), significant differences in the pattern of dissociation are apparent, with an additional 6 m of the deposit dissociated for $k = 10^{-13}$ m^2 compared to the base case; for lower permeability ($k = 10^{-17}$ m^2), there is 40 m of additional undissociated hydrate remaining.

These variations are reflected in the flux of methane at the seafloor (Figure 11), although unlike Case II, all simulated sediment permeabilities result in methane flux in the gas phase at the seafloor. At $k = 10^{-14}$ m^2, methane arrives at the seafloor 4 yr earlier

than in the base case and appears simultaneously in both aqueous and gas phases. Methane fluxes, Q_{CH4}, peak immediately at 2.5 times the base-case maximum instantaneous methane flux—Q_G = 0.5 m^3/yr STP (22.3 mol/yr) of methane gas and Q_{Aq} = 0.035 m^3/yr STP (1.6 mol/yr) of aqueous methane per m^2 of seafloor. For $k = 10^{-13}$ m^2, methane arrives at the seafloor 6 yrs sooner, with 4 times the maximum instantaneous methane flux seen in the base case (Q_G = 0.8 m^3/yr STP or 36 mol/yr and Q_{Aq} = 0.03 m^3/yr STP or 1.3 mol/yr per m^2 of seafloor). These fluxes are maintained at a roughly constant level throughout the 100 yr simulation period for the $k = 10^{-13}$ m^2 and $k = 10^{-14}$ m^2 simulations. Reduced permeability, to $k = 10^{-17}$ m^2, delays the arrival of methane at the seafloor compared to the base case, and results in a maximum methane flux of Q_G = 0.017 m^3/yr STP (0.76 mol/yr) and Q_{Aq} = 0.008 m^3/yr STP (0.36 mol/yr) per m^2 of seafloor.

These results show the importance of coupling heat and mass transport to hydrate thermodynamics in the analysis of the hydrate dissociation process. The rate of dissociation and the rate of methane release are not merely a function of a fixed thermal diffusivity—it is determined by the complex, coupled interaction between heat conduction, advection, transport of heat via the advecting fluid, the heat of dissociation of hydrate, and the amenability of the sediments to liquid and gas transport (as described by the intrinsic permeability, k, and the relationships for capillarity and relative permeability in a multiphase system). Less permeable sediments reduce the rate of dissociation by limiting heat transport via moving fluids, while also restricting the movement of the released gas and therefore causing more gas to be entrained within the sediment column

in the short term. For systems with lower methane flux at the seafloor due to reduced permeability, aqueous phase transport of methane assumes a more dominant role. If longer times are considered, it is expected that transport in aqueous and/or gas phases will eventually allow much of the methane to escape into the ocean environment. A significantly reduced methane flux, particular one limited to aqueous-phase transport, may allow benthic biological processes, not examined here, greater access to the released methane and enhance the possibility of oxidation to CO_2 and/or sequestration within sediments.

Cumulative methane fluxes for Case II and Case III, for all permeabilities, are shown in Figure 12. As expected from the instantaneous flux results, higher permeabilities result in larger total quantities of methane flux at the seafloor for either case. For the base-case permeability and for simulations using increased permeability, the total methane release into the ocean is greater for Case III than Case II, reflecting both the larger instantaneous methane fluxes seen in Figure 11 vs. Figure 9, as well as the much larger quantity of methane stored in the thicker, colder hydrate bearing layer of Case III. However, for the lowest permeability, we see that the cumulative flux for Case II exceeds the cumulative flux for Case III for nearly all of the simulated time, and that the total releases are comparable at t = 100 yr. This reflects the instability of a warmer deposit, prone to more rapid dissociation at early times (for identical $\Delta T_{seafloor}$) despite the larger quantity of hydrate available for dissociation in Case III. Once the initial delay in the initiation of seafloor methane flux is overcome, Case III/10^{-17} m^2 generates similar

methane fluxes to Case II/10^{-17} m^2 and can maintain that flux for much longer periods of time.

Effect of initial hydrate saturation

The baseline assumption of $S_{H0} = 0.03$ used in this study reflects a conservative estimate for widespread stratigraphic hydrate deposits. However, the region of greatest concern, the Arctic may contain richer deposits due to temperature-pressure conditions that promote hydrate formation and hydrate stability, and due to ecological factors. While typical hydrate saturations ocean-wide have been estimated in the range of 1 to 10% (Archer, 2007), increased sediment-surface organic carbon concentrations (Seiter et al., 2004) may lead to higher than average hydrate saturations in regions such as the Arctic continental shelf.

To demonstrate the possible increase in methane release for higher-S_H deposits, we compare the reference Case III to the parallel scenario (Reagan and Moridis, 2007) that used an initial hydrate saturation of $S_{H0} = 0.10$. For this scenario, we re-equilibrate the initial condition to establish the thickness of the GHSZ at a new S_{H0}, and then simulate Case III maintaining all other reference-case parameters and temperature variations. In Figure 13, fluxes for a hydrate deposit with $S_{H0} = 0.03$ dissociating under the influence of $\Delta T_{seafloor}$ = 1, 3, and 5 ^{o}C / 100 yr ranged from 0.18 m^3/yr STP (8 mol/yr) to 0.3 m^3/yr STP (13 mol/yr) per m^2 of seafloor (refer also to Figure 6). Increasing hydrate saturation by more than a factor of 3, to $S_{H0} = 0.10$, results in a factor of 5 to 6 increase in the peak methane flux, reaching 0.86 m^3/yr STP (38 mol/yr) to 1.7 m^3/yr STP

(76 mol/yr) per m^2 of seafloor (Reagan and Moridis, 2007). In Figure 14, cumulative methane release over the 100 yr simulation period increases from 13.5 to 22.4 m^3 STP (600-1000 mol) to 71.7 to 146 m^3 STP (3200-6500 mol) per m^2 of seafloor.

The instantaneous and total fluxes of methane increase significantly with increased initial S_{H0}, but the recession of the upper hydrate boundary proceeds more slowly. Figures 15a and 15b show saturation and temperature profiles for Case III at t = 100 yr for S_{H0} = 0.03 (base case) and S_{H0} = 0.10 (Reagan and Moridis, 2007), respectively. In Figure 15b, the hydrate has receded 38 m, in comparison to 60 m for the base case. This is a consequence of the substantial heat of dissociation for solid hydrate: the larger mass of hydrate per volume of sediment in the higher-S_H deposit requires greater heat input per volume of dissociated hydrate. The temperature profile in Figure 15b exhibits a sharper discontinuity at the location of the dissociation front than in Figure 15a, reflecting this effect. Consequently, deposits with higher S_H can release more methane (due to greater total hydrate mass), and the instantaneous methane fluxes at the seafloor will be greater. The total volume of dissociated hydrate (that is, the change in thickness of the GHSZ) for a given $\Delta T_{seafloor}$ is expected to be similar regardless of initial saturation—however, the time needed to dissociate the full hydrate deposit is lengthened.

Effect of depth within the sediment column

The previous examples focus on the behavior of hydrate deposits assuming an overlying ocean of uniform properties (constant depth, constant salinity), and the fluxes, Q, represent methane flux at the sediment-water boundary for cases where the hydrate

deposit extends from just below the seafloor to the base of the GHSZ. However, due to chemical and biochemical activity, the upper sediment column is often depleted of methane and, consequently, methane hydrate (Borowski et al., 1999). A layer of hydrate-free sediments on top of the methane hydrate deposit separates ocean temperature variations from the hydrate-bearing layers, and may delay the appearance of released methane at the seafloor.

To assess the effect of deposit depth, we compare the scenarios described in the previous section (Case III, 320 m seafloor depth, S_{H0} = 0.03 and 0.10, $k = 10^{-15}$ m^2, $\Delta T_{seafloor}$ = 3 ^{o}C) to a hydrate system with the top of the deposit located 30 m below the seafloor (mbsf). The top 30 m of hydrate was removed, and the system was re-equilibrated to insure a realistic gradient of dissolved methane (Borowski, 1999) in the hydrate-free zone between the top of the deposit and the methane-free overlying ocean. The simulation parameters and method were otherwise identical to Case III.

Methane fluxes for the reference Case III vs. a 30 mbsf deposit are compared in Figure 16. (To accommodate longer timescales and the inherent uncertainty of estimating temperature change past 100 yr, the figure has been extended to t = 400 yr total time, with the temperature held constant for 100 yr < t < 400 yr) The 30 m of overlying sediment significantly delays the onset of methane flux at the seafloor for deposits with S_H = 0.03 and S_H = 0.10. For Case III, S_H = 0.03, we see the arrival of aqueous and gaseous methane at t = 11 yr. Removing the top 30 m of hydrate results in no methane flux at the seafloor until t = 60 yr, and then only as dissolved methane, Q_{Aq} = 0.029 m^3/yr

STP (1.3 mol/yr) per m^2 of seafloor. For $S_H = 0.10$, removing the top 30 m of hydrate results in a 90-yr delay before the gaseous methane reaches the seafloor. For $t > 90$ yr, methane fluxes for both cases are quite similar (a difference of less than 0.1 $m^3/yr/m^2$ STP or 4.5 $mol/yr/m^2$). The time axis in Figure 16 is extended beyond the 100-yr limit of previous graphs to illustrate this further evolution—the temperature at the top of the sediment column is held constant at the elevated (+3 ^oC) temperature beyond $t = 100$ yr.

The effect of overlying sediments is limited to a delay in the arrival of the temperature disturbance at the top of the hydrate zone and a corresponding delay in the arrival of released methane at the seafloor. Once the hydrate begins to dissociate, the same localized front forms at the top of the deposit and the rate of hydrate dissociation is similar. Once the sediment column fills with the released methane beyond the irreducible gas saturation of the porous medium, the net rate of methane transport to the seafloor is essentially the same and regulated by the permeability of the sediment. On a timescale of hundreds or thousands of years, any persistent temperature change will eventually shift the extent of the GHSZ, resulting in dissociation of the hydrate deposit for all cases investigated here. The rapidity of methane release into the environment will be tied to the coupled processes of hydrate dissociation, and heat and mass transport.

Effect of sea level changes

One predicted consequence of climate change is that sea levels may rise due to melting of terrestrial ice deposits, with estimates ranging from 0.09 - 0.88 m by the year 2100 (IPCC, 2001) with much larger increases possible if CO_2 emissions continue

unabated. Increasing the depth of the ocean increases the pressure at the seafloor, potentially stabilizing oceanic hydrate deposits. Increased pressure at the seafloor, with geothermal gradients and ocean temperature profiles held constant, would lower the bottom of the GHSZ and raise the top of the GHSZ, creating a larger window of hydrate stability and altering the effects of a given ΔT. To quantify this effect, we compare Case III to two parallel cases, setting P_0 = 32.1 bar and P_0 = 33 bar for fixed pressure at the top of the sediment column, corresponding to increases in ocean depth of roughly Δz = +1 m (similar to IPCC estimates) and Δz = +10 m (a case of extreme, possibly catastrophic sea level rise). All other simulation parameters are maintained at reference values. Thermal expansion of the ocean due to global temperature changes (which would not alter seafloor pressure) is not considered—the density of the overlying ocean is assumed to remain constant.

Figure 17 compares methane fluxes for the base Case III vs. the evolution of fluxes for conditions of increased sea level. As expected, the stabilizing effect of increased pressure reduces the magnitude of Q_{CH4} and delays the release of methane into the ocean for all ΔT scenarios. For Δz = +1 m, the stabilization is minimal, with the appearance of methane at the seafloor delayed by no more than Δt = +2 yr (ΔT = 1 ^{o}C / 100 yr), and only minor reductions in the flux of methane out of the sediment. Under the extreme case of Δz = +10 m, some attenuation occurs. For the largest temperature increase of ΔT = 5 ^{o}C / 100 yr, we see a delay of Δt = +8 yr in the appearance of methane at the seafloor and a reduction in peak Q_{CH4} of 12%. In contrast, for ΔT = 1 ^{o}C / 100 yr, the effect is considerably greater, with a delay of Δt = +33 yr and a 24% reduction in peak Q_{CH4}. While very large changes in ocean depth may mitigate, somewhat, methane

release due to warming at the seafloor, even such an immediate, large (possibly catastrophic) increase in sea level merely delays and attenuates methane fluxes without preventing dissociation and release of methane.

Conclusions

In this study we assess the stability of three types of hydrates—deep, cold deposits in the deep oceans; shallow, warm deposits, as found in the Gulf of Mexico; and shallow, cold deposits, representative of the Arctic continental shelf—and simulate the dynamic behavior of these deposits under the influence of moderate ocean temperature increases. We reach the following conclusions for simple, initially steady-state, uniform, stratigraphic hydrate deposits:

1) Deep, cold hydrates (Case I) are stable under the influence of moderate increases in ocean temperature over short time scales. This agrees with previous equilibrium thermodynamic models of hydrate formation, dissociation, and redistribution, and suggests again that deep hydrates, although quite prevalent, are not of immediate concern to climate modelers.

2) Shallow hydrates (located at or near the top of the GHSZ) can be very unstable, and produce significant gaseous and dissolved methane within seafloor sediments under the influence of as little as 1 ^{o}C of seafloor temperature increases (Cases II and III).

3) The permeability of ocean sediments affects the rate of hydrate dissociation, the rate of methane transport to the seafloor, and the ratio of gaseous methane to aqueous methane in the net methane flux. However, the shift in the position of the top and bottom of the GHSZ due to temperature variations remains, and therefore low permeabilities affect only the transport of the released methane, not the stability of the hydrate deposit itself.

4) Higher-saturation deposits produce larger methane fluxes, while the thermodynamics of hydrate dissociation retards the rate of recession of the upper hydrate interface. Again, the change in the location of the GHSZ is primarily a function of temperature and pressure alone, and changes in saturation change the quantity of methane produced, the flux of methane at the seafloor, and the length of time required to dissociate the hydrate formation.

5) Increasing hydrate depth with the sediment column delays both the onset of dissociation and the arrival of methane at the seafloor, however, the magnitude of the peak methane flux is similar, with the evolution of methane flux at the seafloor shifted in time.

6) Similarly, increases in sea level can delay the arrival of methane at the seafloor and attenuate the peak methane flux, however the stabilizing effect is not sufficient to prevent methane release.

7) The results suggest that rapid release of methane is possible for shallow hydrates in warm and cold regions, and that arctic hydrates, if found to be as widespread as some evidence suggests, may present a particular threat to regional or global ecology. Application of these results as a source term to ocean and climate models can answer important questions about the role of hydrate-derived methane in global climate cycles.

Acknowlegements

This research has been supported by the Laboratory Directed Research and Development (LDRD) program at Lawrence Berkeley National Laboratory, by the Director, Office of Science, of the U.S. Department of Energy (DoE) under Contract No. DE-AC02-05CH11231, and by the Assistant Secretary for Fossil Energy, Office of Natural Gas and Petroleum Technology, through the National Energy Technology Laboratory (NETL). The authors would like to thank John Apps, Yongkoo Seol, and Scott Elliott for their insightful reviews and comments.

References

Archer, D. (2007), Methane hydrate stability and anthropogenic climate change, *Biogeosciences*, *4*, 521-544.

Archer, D., and Buffett, B. (2005), Time-dependent response of the global ocean clathrate reservoir to climatic and anthropogenic forcing. *Geochem. Geophys. Geosys.*, *6*(3), Q03002, doi:10.1029/2004GC000854.

Boetius, A., and Suess (2004), E. Hydrate Ridge: a natural laboratory for the study of microbial life fueled by methane from near-surface gas hydrates. *Chemical Geology, 205*, 291-310.

Borowski, W.S., Paull, C.K., and Ussler, W. (1999), Global and local variations of interstitial sulfate gradients in deep-water, continental margin sediment: Sensitivity to underlying methane and gas hydrates. *Marine Geology*, *159*, 131-154.

Borowski, W.S. (2004), A review of methane and gas hydrates in the dynamic, stratified system of the Blake Ridge region, offshore southeastern North America. *Chem. Geology, 205*, 311-346.

Brook, E.J., Sowers, T., and Orlando, J. (1996), Raid variations in atmospheric methane concentration during the past 110,000 years. *Science, 273*, 1087-1091.

Brewer, P.G., Paull, C., Peltzer, E.T., Ussler, W., Rehder, G., and Friederich, G. (2002), Measurements of the fate of gas hydrates during transit through the ocean water column *Geophys. Res. Lett.*, *29*(22), doi:10.1029/2002GL014727.

Buffett, B., and Archer, D. (2004), Global inventory of methane clathrate: Sensitivity to changes in environmental conditions. *Earth Planetary Sci. Lett., 227*, 185-199.

Circone, S., Kirby, S.H., and Stern, L. (2005), Direct Measurement of Methane Hydrate Composition along the Hydrate Equilibrium Boundary. *J. Phys. Chem. B*, *109*(19), 9468-9475.

Collett, T.S., and Kuuskraa, V.A. (1998), Hydrates contain vast store of world gas resources, *Oil and Gas Journal*, *96*(19), 90-95.

Dickens, G.R., O'Neil, J.R., Rea, D.K., and Owens, R.M. (1995), Dissociation of oceanic methane hydrate as a cause of the carbon isotope excursion at the end of the Paleocene. *Paleoceanography, 10*, 965-971.

Dobrynin, V.M., Korotajev, Y.P., and Plyuschev, D.V. (1981), in *Long-Term Energy Resources*, R. F. Meyer and J. C. Olson, Eds., Pitman: Boston, Mass.

Ginsburg, G.D. and Soloviev, VA. (1998), *Submarine Gas Hydrates*. St. Petersburg.

Gornitz V., and Fung, I. (1994) Potential distribution of methane hydrate in the world's oceans. *Global Biogeochem. Cycles, 8*, 335-347.

Holbrook, W.S., Hoskins, H., Wood, W.T., Stephen, R.A., and Lizarralde, D. (1996), Methane hydrate and free gas on the Blake Ridge from vertical seismic profiling. *Science, 273*, 1840-1843.

Hornbach, M.J., Saffer, D.M., and Holbrook, W.S. (2004), Critically pressured free-gas reservoirs below gas-hydrate provinces, *Nature*, 427, 142-144.

Hovland, M., Svensen, H., Forsberg, C.F., Johansen, H., Fichler, C., Fossa, J.H., Jonsson, R., and Rueslatten, H. (2005), Complex pockmarks with carbonate-ridges off mid-Norway: Products of sediment degassing. *Marine Geology, 218,* 191-206.

IPCC, Ed. (2001), *Climate Change 2001: The Scientific Basis. Contribution of Working Group I to the Third Assessment Report of the Intergovernmental Panel on Climate Change*, Cambridge Univ. Press, Cambridge, UK.

Kennedy, M., Mrofka, D., and von der Borch, C. (2008), Snowball Earth termination by destabilization of equatorial permafrost methane clathrate, *Nature*, *453*, 642-645.

Kennett, J.P., and Stott, L.D. (1991), Abrupt deep-sea warming, palaeoceanographic changes and benthic extinctions at the end of the Palaeocene, *Nature*, *353*, 225-229.

Kennett, J.P., Cannariato, K.G., Hendy, L.L., and Behl, R.J. (2000), Carbon isotopic evidence for methane hydrate instability during quaternary interstadials. *Science, 288*, 128-133.

Kennett, J.P., Cannariato, K.G., Hendy, L.L., and Behl, R.J. (2002), *Methane hydrates in quaternary climate change: The Clathrate Gun Hypothesis*, AGU Publishing, Washington, DC.

Klauda, J.B., and Sandler, S.I. (2005) Global distribution of methane hydrate in ocean sediment. *Energy and Fuels, 19*, 459-470.

Kvenvolden, K.A. (1988), Methane hydrates and global climate, *Global Biochemical Cycles*, *2*, 221-229.

Kvenvolden, K.A. (1999), Potential effects of gas hydrate on human welfare. *Proc. Nat. Acad. Sci., 96*, 3420-3426.

Luff, R., Greinert, J., Wallmann, K., Klaucke, I., and Suess, E. (2005), Simulation of long-term feedbacks from authigenic carbonate crust formation at cold vent sites. *Chemical Geology, 216*, 157-174.

Makagon, Y.F. (1974), *Hydrates of natural gas* (translated from the Russian), PennWell Books, Tulsa, OK.

Meehl, G., T.F. Stocker, Collins, W.D., and 12 others (2007), Global climate projections, In: *Climate Change 2007: The Physical Basis*, In *IPCC AR4*, Cambridge University Press.

Milkov, A.V. (2004), Global estimates of hydrate-bound gas in marine sediments: how much is really out there? *Earth Science Reviews, 66*, 183-197.

Milkov, A.V., and Sassen, R. (2001), Estimate of gas hydrate resource, northwestern Gulf of Mexico continental slope. *Marine Geology, 179*, 71-83.

Milkov, A.V., and Sassen, R. (2003), Two-dimensional modeling of gas hydrate decomposition in the northwestern Gulf of Mexico: Significance to global change assessment. *Global and Planetary Change 36*, 31-46.

Moridis, G.J. (2002), Numerical Simulation Studies of Thermally-Induced Gas Production From Hydrate Accumulations With No Free Gas Zones at the Mallik Site, Mackenzie Delta, Canada, *SPE 77861,* presented at the SPE 2002 Asia Pacific Oil and Gas Conference and Exhibition, Melbourne, Australia, October 8-10, 2002.

Moridis, G.J. (2003), Numerical studies of gas production from methane hydrates, SPE-87330, *SPE Journal*, Dec. 2003, 359-370.

Moridis, G.J., Collett, T., Dallimore, S., Satoh, T., Hancock, S., and Weatherhill, B. (2004), *J. Petroleum Science and Engineering*, *43*, 219-239.

Moridis, G.J., and Kowalsky, M.B. (2005), Gas Production from Unconfined Class 2 Hydrate Accumulations in the Oceanic Subsurface, in *Economic Geology of Natural Gas Hydrates*, M. Max, A.H. Johnson, W.P. Dillon, and T. Collett, Editors, Kluwer Academic/Plenum Publishers.

Moridis, G.J., Collett, T.S., Dallimore, S.R., Inoue, T., and Mroz, T. (2005a), Analysis and Interpretation of the Thermal Test of Gas Hydrate Dissociation in the

JAPEX/JNOC/GSC et al. Mallik 5L-38 Gas Hydrate Production Research Well, in *Geological Survey of Canada, Bulletin, 585*, S.R. Dallimore and T. Collett, Eds.

Moridis, G.J., Seol, Y., Kneafsey, T. (2005b), Studies of reaction kinetics of methane hydrate dissociation in porous media (Paper 1004), Proceedings of the 5th International Conference on Gas Hydrates, Trondheim, Norway, 12-16 June 2005.

Moridis, G.J., and Kowalsky, M.B. (2007), Response of Oceanic Hydrate-Bearing Sediments to Thermal Stresses, OTC 18193, *SPE Journal*, *12*(2), 253-268, doi:10.2118/111572-PA.

Moridis, G.J., and Reagan, M.T. (2007a), Strategies for Gas Production From Oceanic Class 3 Hydrate Accumulations, OTC 18865, Proceedings, 2007 Offshore Technology Conference, Houston, Texas, USA, 30 April - 3 May 2007.

Moridis, G.J., and Reagan, M.T. (2007b), Gas Production From Oceanic Class 2 Hydrate Accumulations, OTC 18866, Proceedings of the 2007 Offshore Technology Conference, Houston, Texas, USA, 30 April - 3 May 2007.

Moridis G.J. and Sloan, E.D. (2007), Gas production potential of disperse low-saturation hydrate accumulations in oceanic sediments. *Energ. Convers. Manag.*, *48*, 1834-1849.

Moridis, G.J., Kowalsky, M.B. and Pruess, K. (2007), Depressurization-Induced Gas Production From Class 1 Hydrate Deposits, OTC 97266, *SPE Reservoir Evaluation and Engineering*, *10*(5), 458-488.

Moridis, G.J., Kowalsky, M.B., and Pruess, K. (2008), TOUGH+HYDRATE v1.0 User's Manual: A Code for the Simulation of System Behavior in Hydrate-Bearing Geologic Media. *Report LBNL-0149E*, Lawrence Berkeley National Laboratory, Berkeley, CA.

1 Nisbet, E.G. (2002), Have sudden large releases of methane from geological reservoirs
2 occurred since the Last Glacial Maximum, and could such releases occur again? *Phil.*
3 *Trans, R. Soc. Lond., A. 360*, 581-607.

4 O'Hara, K. D. (2008), A model for late Quaternary methane ice core signals: Wetlands
5 versus a shallow marine source, *Geophys . Res. Lett*., *35*, L02712, doi:10.1029/
6 2007GL032317.2.1.

7 Reagan, M.T. and Moridis, G.J. (2007), Oceanic gas hydrate instability and dissociation
8 under climate change scenarios, *Geophys. Res. Lett.*, *34*, L22709, doi: 10.1029/
9 2007GL031671.

10 Rothwell, R.G., Thomson, J., and Kahler, G. (1998), Low-sea-level emplacement of a
11 very large Late Pleistocene 'megaturbidite' in the western Mediterranean Sea, *Nature*,
12 *392*, 377-380.

13 Ruppel, C., Dickens, G.R., Castellini, D.G., Gilhooly, W., and Lizarralde, D. (2005),
14 Heat and salt inhibition of gas hydrate formation in the northern Gulf of Mexico,
15 *Geophys. Res. Lett.*, *32,* L04605, doi: 10.1029/2004GL021909.

16 Rutqvist, J., and Moridis, G.J. (2007), Numerical Studies of Geomechanical Stability of
17 Hydrate-Bearing Sediments, OTC 18860, Proceedings, 2007 Offshore Technology
18 Conference, Houston, Texas, USA, 30 April - 3 May 2007.

19 Sassen, R., Joye, S., Sweet, S.T., DeFreitas, D.A., Milkov, A.V., and MacDonald, I.R.
20 (1999), Thermogenic gas hydrates and hydrocarbon gases in complex chemosynthetic
21 communities, Gulf of Mexico continental slope. *Organic Geochemistry, 30*, 485-497.

1 Seiter, K., Hensen, C., Schroter, J., and Zabel, M. (2004), Organic carbon content in
2 surface sediments—defining regional provinces, *Deep-Sea Research I*, *51*, 2001-2026.

3 Severinghaus, J.P., Sowers, T., Brook, E.J., Alley, R.B., and Bender, M.L. (1998),
4 Timing of abrupt climate change at the end of the Younger Dryas interval from
5 thermally fractionated gases in polar ice. *Nature, 391*, 141-146.

6 Sloan, E.D. (1998), *Clathrate Hydrates of Natural Gases*, Marcel Decker, Inc., New
7 York, NY.

8 Sowers, T. (2006), Late quaternary atmospheric CH_4 isotope record suggests marine
9 clathrates are stable. *Science, 311*, 838-840.

10 Spinelli, G.A., Giambalvo, E.R., and Fisher, A.T. (2004), Sediment permeability,
11 distribution, and influence on fluxes in oceanic basement. *Hydrogeology of the Oceanic*
12 *Lithosphere*, E.E. Davis and H Elderfield, Eds. Cambridge University Press.

13 Stone, H.L. (1970), Probability model for estimating three-phase relative permeability,
14 *Trans. SPE AIME*, *249*, 214-218.

15 Tang, L-G, Li, X-S, Feng, Z-P, Li, G., and Fan, S-S (2007) Control mechanisms for gas
16 hydrate production by depressurization in different scale hydrate reservoirs, *Energy &*
17 *Fuels*, *21*, 227-233.

18 Valentine, D.L., Blanton, D.C., Reeburgh, W.S., and Kastner, M. (2001), Water column
19 methane oxidation adjacent to an area of active hydrate dissociation, Eel River Basin,
20 *Geochim Cosmochim. Acta*, *65*, 16, 2633-2640.

21 Van Genuchten, M.T. (1980), A closed-form equation for predicting the hydraulic
22 conductivity of unsaturated soils, *Soil Sci. Soc.*, *44*, 892-898.

Xu, W. and Ruppel, (1999), Predicting the occurrence, distribution, and evolution of methane gas hydrate in porous marine sediments, *J. Geophys. Res.*, *104*, B3, 5081-5095.

Xu, W., and Lowell, R.P. (2001), Effect of seafloor temperature and pressure variations on methane flux from a gas hydrate layer: Comparison between current and late Paleocene climate conditions. *J. Geophys. Res.*, *106*, B11, 26413-26423.

List of Captions

Figure 1: Pressure-temperature equilibrium of the simple methane hydrate system as used in TOUGH+HYDRATE (Moridis et al., 2008). Phases shown are liquid water (Lw), gaseous phase (V), solid hydrate (H), and solid ice (I). The Lw-H region is the hydrate stability region relevant to oceanic hydrates.

Figure 2: Schematic of the gas hydrate stability zone in the seafloor environment (not to scale). In this example, the top of the gas hydrate stability zone (GHSZ) is above the seafloor; however, the boundary may exist above, at, or below the seafloor depending on local pressure and temperature conditions. Increasing temperatures (temperature profile 1 to temperature profile 2) lowers the position of the top of the GHSZ (A) and raises the position of the bottom of the GHSZ (B), as the zone of hydrate stability is defined by the intersection of the temperature profile with the phase envelope.

Table 1: Physical properties parameters for the hydrate-bearing sediment system.

Figure 3: Profiles of hydrate and gas saturation, with temperature, for a 1000 m system undergoing a 3^{o}C increase over 100yr. Panel a) shows the initial, equilibrium profiles at t = 0 yr, panel b1) shows the profiles after 100 yrs of temperature change, and panel b2) shows T and P profiles at t = 100 yr.

Figure 4: Profiles of hydrate and gas saturation, with temperature, for 570 m system undergoing a 3^{o}C increase over 100yr (Reagan and Moridis, 2007) at a) t = 0 yr, b) t = 10 yr, and c) t = 100 yr.

Figure 5: Profiles of hydrate and gas saturation, with temperature, for a 320 m system undergoing a 3^{o}C increase over 100yr, at a) t = 0 yr, b) t = 10 yr, and c) t = 100 yr.

Figure 6: Rates of methane flux per m^2 of seafloor for Case II and Case III undergoing 1, 3, and 5 ^{o}C increases. Methane flux is presented as both m^3 at STP, and in molar units. Case II results are identical to those reported in Reagan and Moridis (2007).

Figure 7: Cumulative methane release per m^2 of seafloor for Case II and Case III systems undergoing 1, 3, and 5 ^{o}C increases over 100 yr. Case II results are identical to those reported in Reagan and Moridis (2007).

Figure 8: Profiles of hydrate and gas saturation (S_H and S_G) at t = 10 yr and t = 100 yr, plus the P profiles at t = 10 yr, for systems with permeabilities k = 10^{-13}, 10^{-15}, and 10^{-17} m^2, for Case II undergoing a 3 ^{o}C increase over 100 yr.

Figure 9: Variation of methane flux with sediment permeability for Case II undergoing a 3 ^{o}C increase over 100 yr. Aqueous methane fluxes are represented by dotted lines, gas flux by solid lines.

Figure 10: Profiles of S_H and S_G at t = 10 yr and t = 100 yr, plus the P profiles at t = 10 yr, for systems with permeabilities $k = 10^{-13}$, 10^{-15}, and 10^{-17} m^2, for Case II undergoing a 3 ^{o}C increase over 100 yr.

Figure 11: Variation of methane flux with sediment permeability, for Case III undergoing a 3 ^{o}C increase over 100 yr. Aqueous methane fluxes are represented by dotted lines, gas fluxes by solid lines.

Figure 12: Cumulative methane release vs. depth and sediment permeability, for Case II and Case III systems undergoing a 3 ^{o}C increase over 100 yr.

Figure 13: Variation of methane flux with initial hydrate saturation for Case III undergoing a 3^{o}C increase over 100 years.

Figure 14: Cumulative methane release vs. initial hydrate saturation for Case III systems undergoing 1, 3, and 5 ^{o}C increases over 100 years.

Figure 15: Profiles of hydrate and gas saturation, with temperature, for Case III at S_H = 0.03 and an elevated initial saturation of S_H = 0.10, after undergoing a 3^{o}C increase over 100yr.

Figure 16: Variation of methane flux with depth of the top of the hydrate deposit for Case III, with S_H = 0.03 and S_H = 0.10, undergoing a 3^{o}C increase over 100 years.

Figure 17: Variation of methane flux with sea level (depth of the overlying ocean) for Case III (S_H = 0.03) undergoing 1, 3, and 5 ^{o}C increases over 100 years.

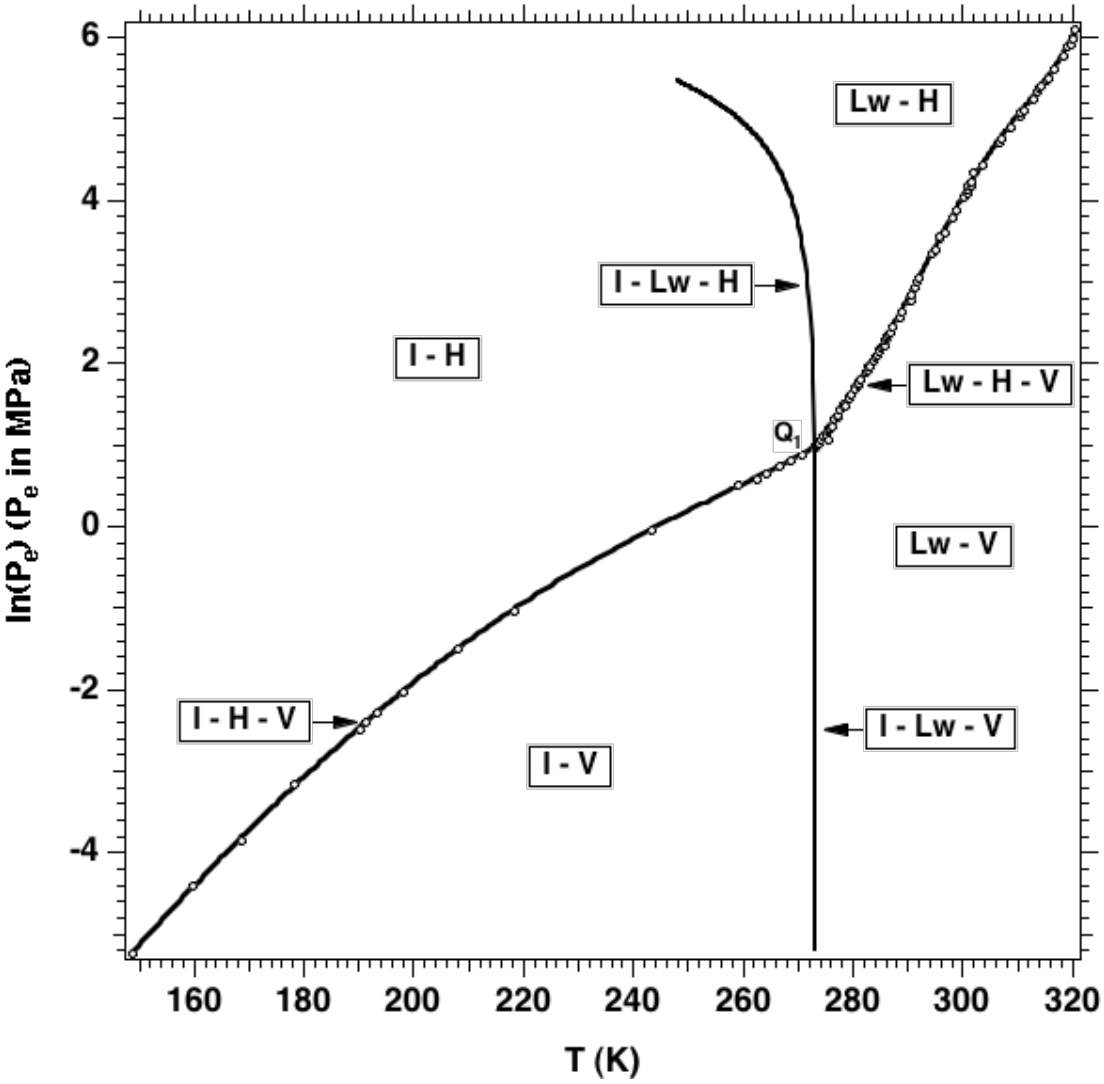

Figure 1: Pressure-temperature equilibrium of the simple methane hydrate system as used in TOUGH+HYDRATE (Moridis et al., 2008). Phases shown are liquid water (Lw), gaseous phase (V), solid hydrate (H), and solid ice (I). The Lw-H region is the hydrate stability region relevant to oceanic hydrates.

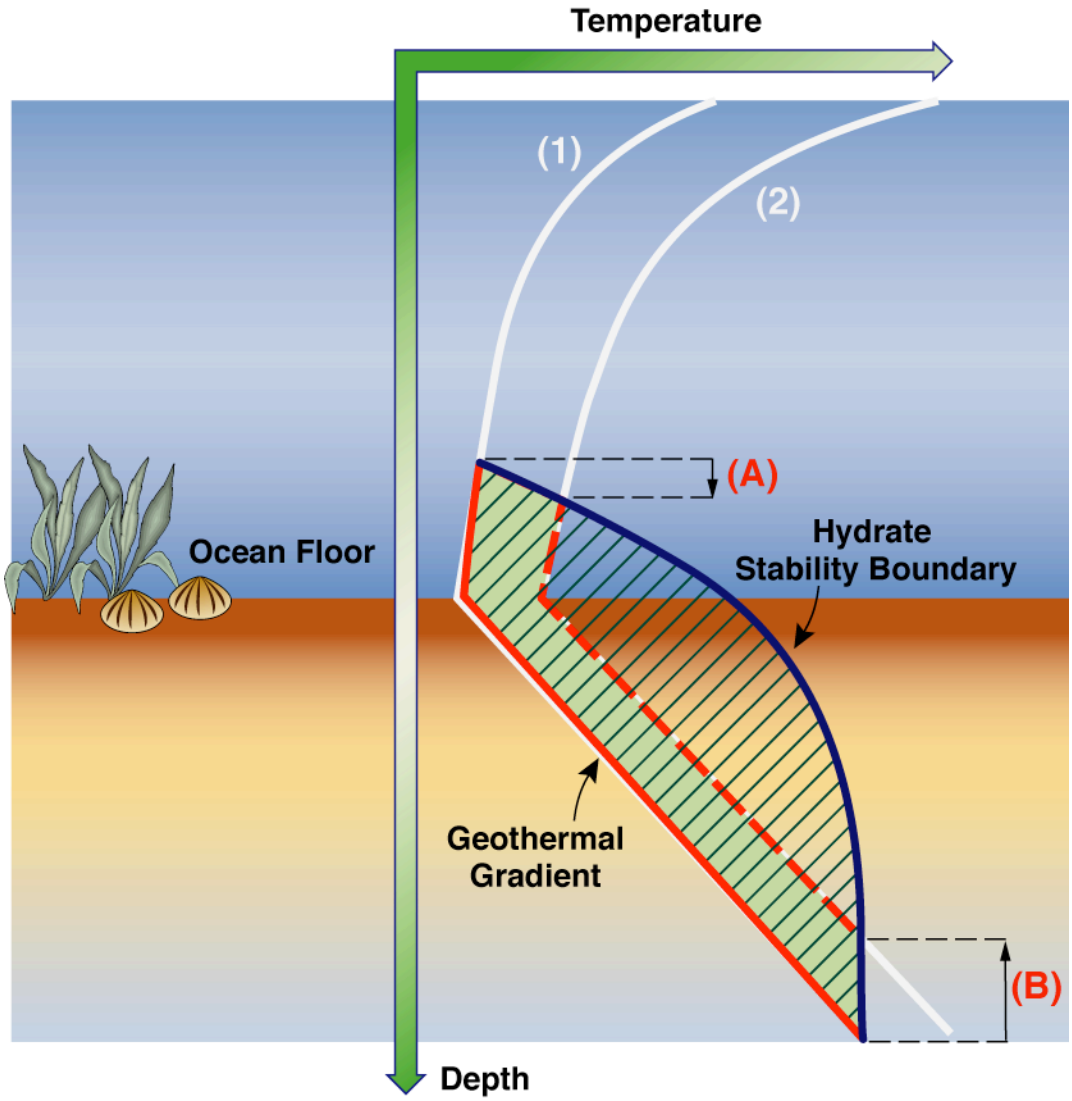

Figure 2: Schematic of the gas hydrate stability zone in the seafloor environment (not to scale). In this example, the top of the gas hydrate stability zone (GHSZ) is above the seafloor; however, the boundary may exist above, at, or below the seafloor depending on local pressure and temperature conditions. Increasing temperatures (temperature profile 1 to temperature profile 2) lowers the position of the top of the GHSZ (A) and raises the position of the bottom of the GHSZ (B), as the zone of hydrate stability is defined by the intersection of the temperature profile with the hydrate stability boundary.

Parameter	Value
Initial salt mass fraction in the ocean and pore water X_0	0.035
Gas composition	100% CH_4
Permeability k	10^{-14} - 10^{-17} m^2 (= 0.01 mD - 10 mD)
Porosity ϕ	0.30
Dry thermal conductivity k_{Sd}	1.0 W/m/K
Wet thermal conductivity k_{Sw}	3.3 W/m/K
Composite thermal Conductivity k_Θ model: Moridis et al. (2005b)	$k_\Theta = (\sqrt{S_H} + \sqrt{S_A})\,(k_{Sw} - k_{Sd}) + k_{Sd}$
Capillary pressure model: Van Genuchten (1980)	$P_{cap} = -P_0\left[\left(S^*\right)^{-1/\lambda} - 1\right]^{-\lambda}$ $S^* = \frac{\left(S_A - S_{irA}\right)}{\left(S_{mxA} - S_{irA}\right)}$
S_{irA}	0.19
P_0	2000 Pa
λ	0.45
Relative permeability model: Modified Stone (1970)	$k_{rA} = (S_A^*)^n$ $k_{rG} = (S_G^*)^n$ $S_A^* = (S_A - S_{irA})/(1 - S_{irA})$ $S_G^* = (S_G - S_{irG})/(1 - S_{irA})$
n	4
S_{irG}	0.02
S_{irA}	0.20

Table 1: Physical properties parameters for the hydrate-bearing sediment system.

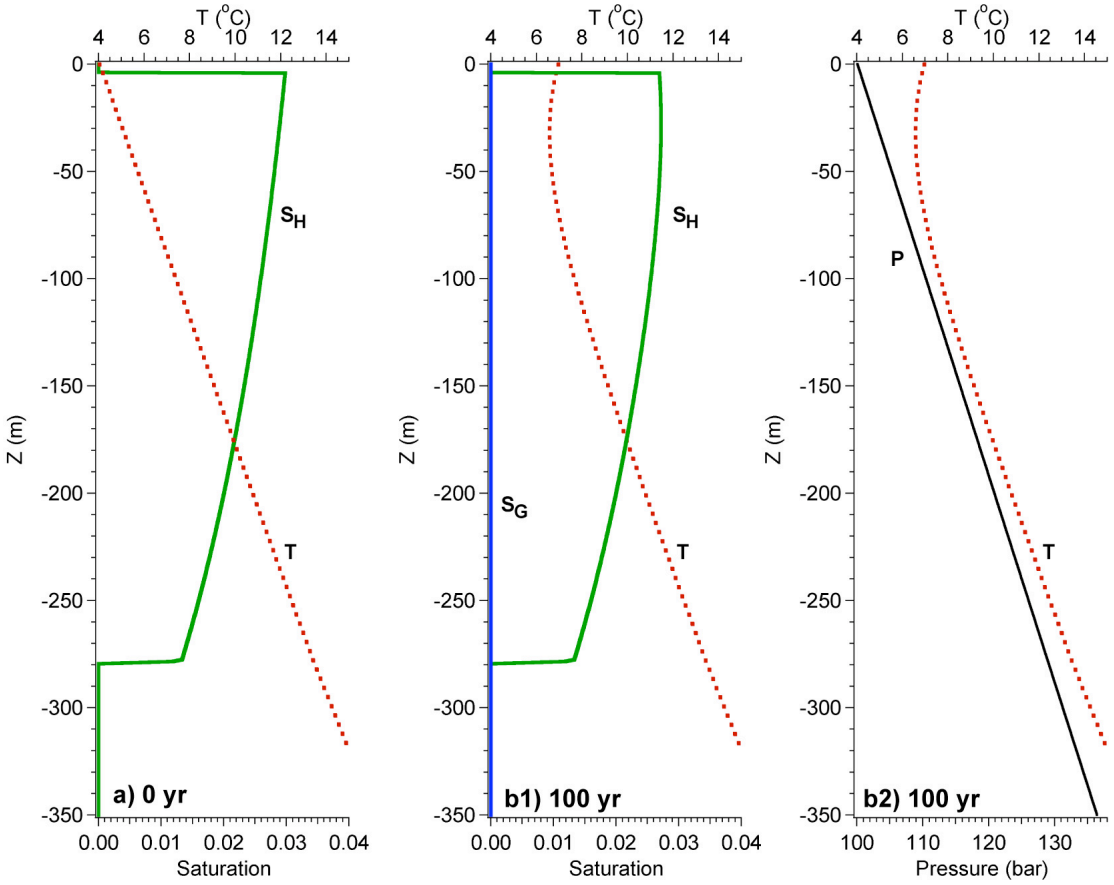

Figure 3: Profiles of hydrate and gas saturation, with temperature, for a 1000 m system undergoing a 3°C increase over 100yr. Panel a) shows the initial, equilibrium profiles at $t = 0$ yr, panel b1) shows the profiles after 100 yrs of temperature change, and panel b2) shows T and P profiles at $t = 100$ yr.

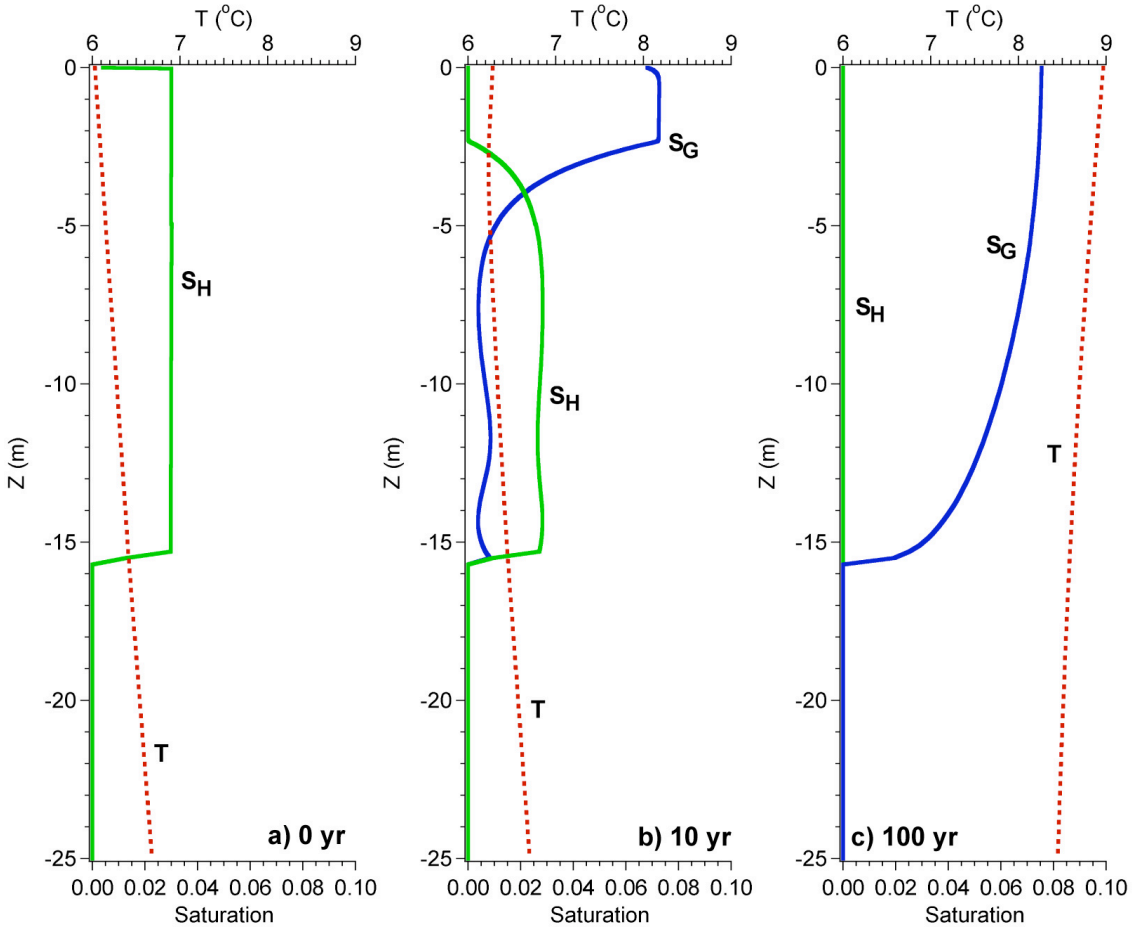

Figure 4: Profiles of hydrate and gas saturation, with temperature, for 570 m system undergoing a 3°C increase over 100yr (Reagan and Moridis, 2007) at a) t = 0 yr, b) t = 10 yr, and c) t = 100 yr.

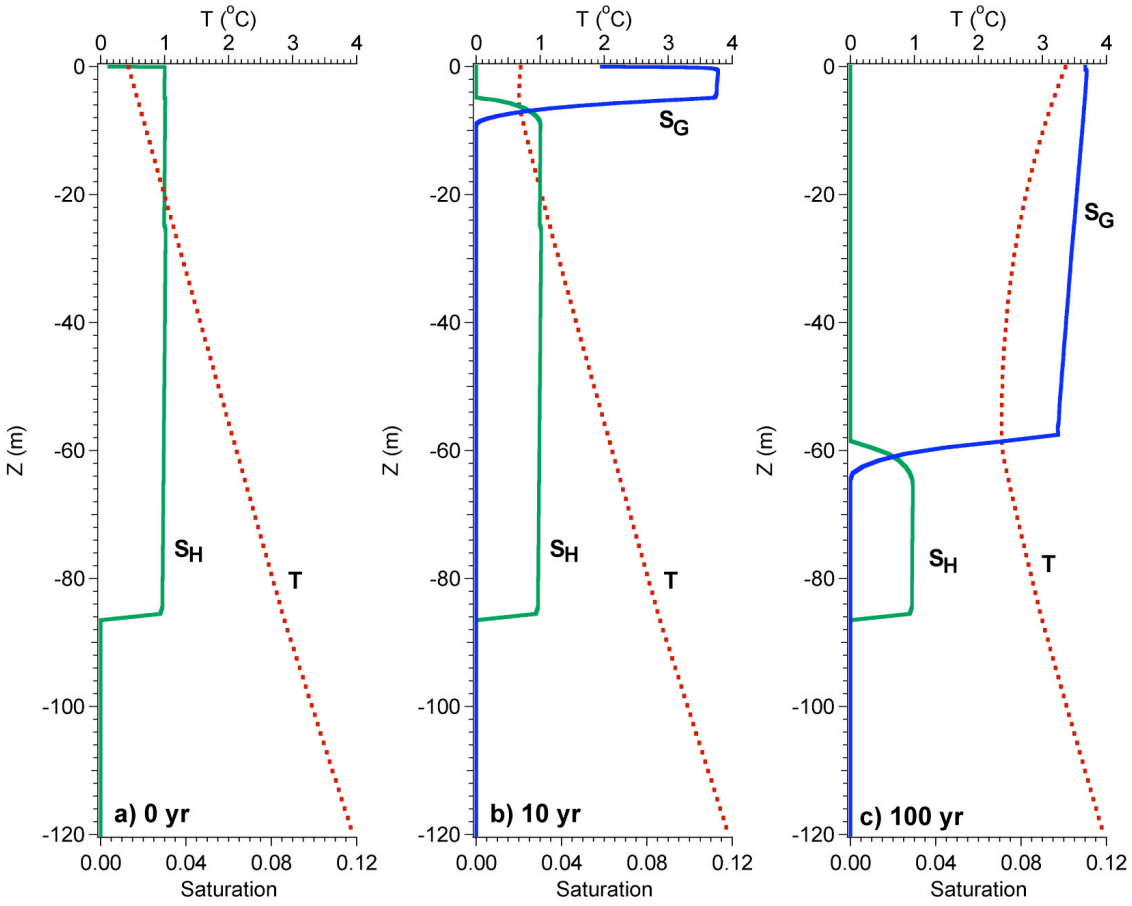

Figure 5: Profiles of hydrate and gas saturation, with temperature, for a 320 m system undergoing a 3°C increase over 100yr, at a) t = 0 yr, b) t = 10 yr, and c) t = 100 yr.

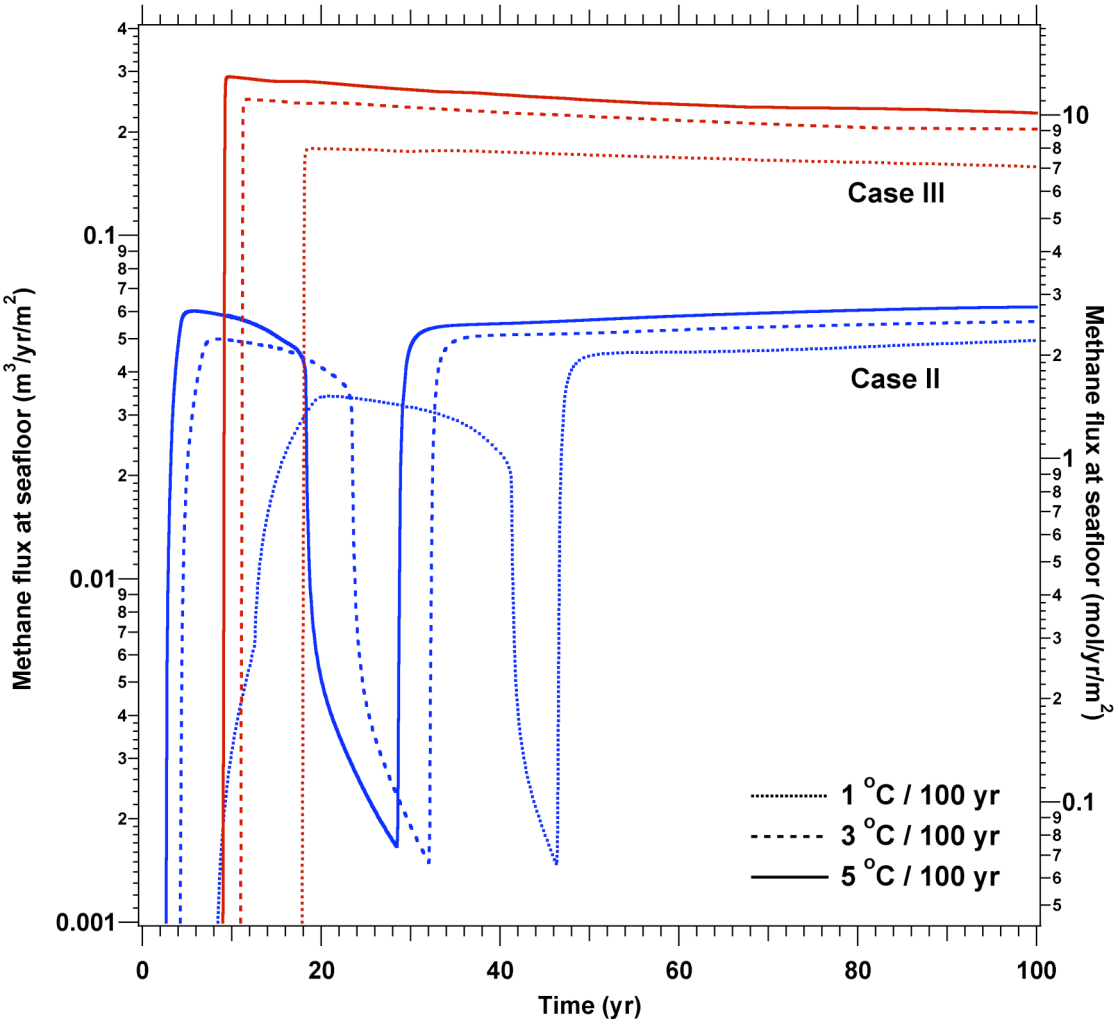

Figure 6: Methane flux per m^2 of seafloor for Case II and Case III undergoing 1, 3, and 5 ^{o}C increases. Methane flux is presented as both m^3 at STP, and in molar units. Case II results are identical to those reported in Reagan and Moridis (2007).

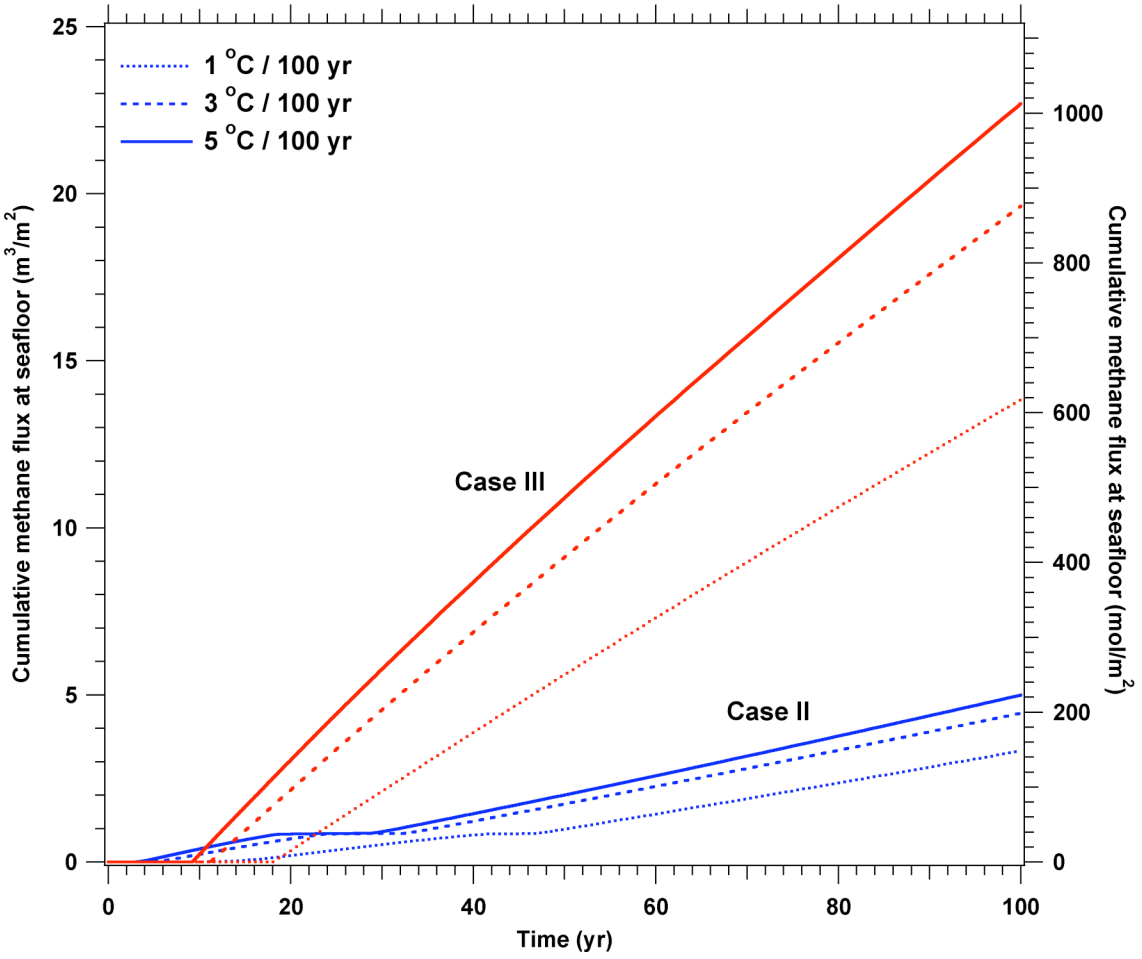

Figure 7: Cumulative methane release per m^2 of seafloor for Case II and Case III systems undergoing 1, 3, and 5 ^{o}C increases over 100 yr. Case II results are identical to those reported in Reagan and Moridis (2007).

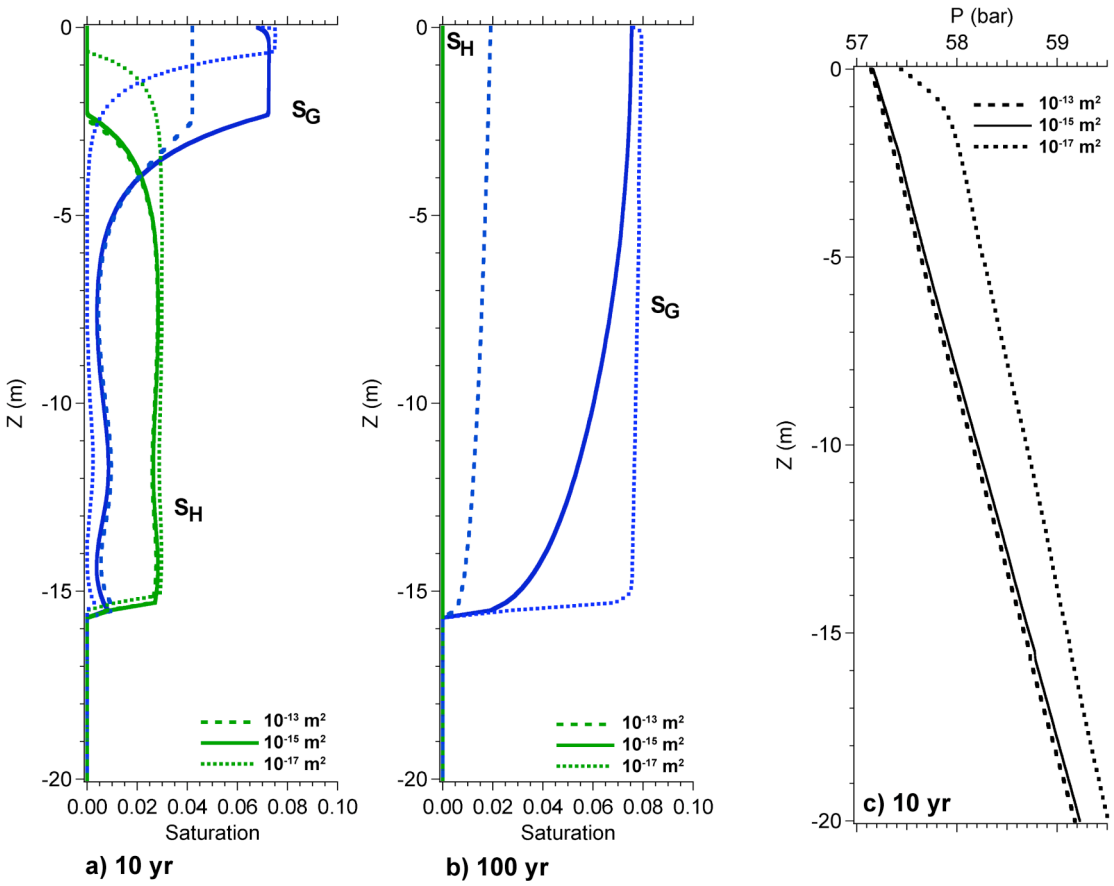

Figure 8: Profiles of hydrate and gas saturation (S_H and S_G) at t = 10 yr and t = 100 yr, plus the P profiles at t = 10 yr, for systems with permeabilities $k = 10^{-13}$, 10^{-15}, and 10^{-17} m^2, for Case II undergoing a 3 ^{o}C increase over 100 yr.

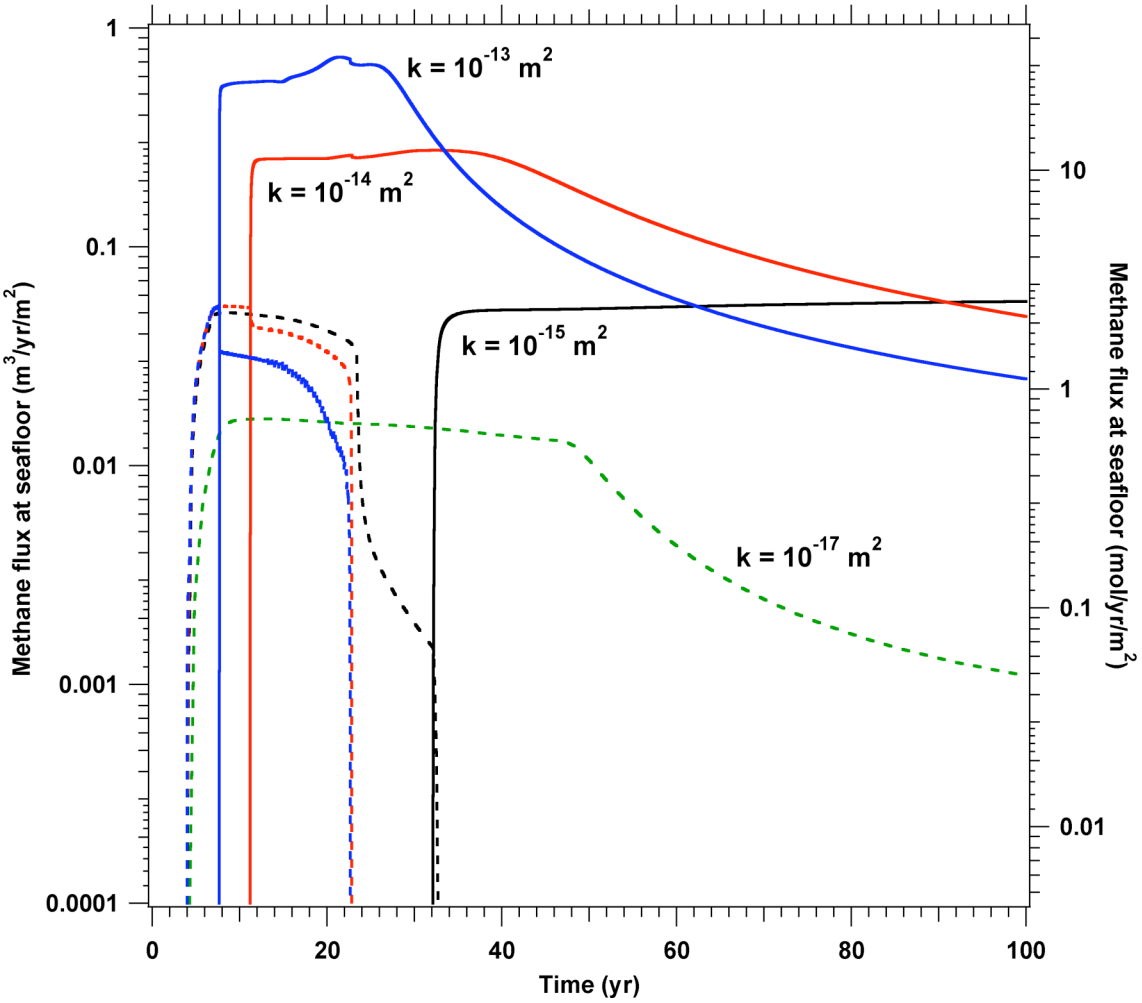

Figure 9: Variation of methane flux with sediment permeability for Case II undergoing a 3 ^{o}C increase over 100 yr. Aqueous methane fluxes are represented by dotted lines, gas flux by solid lines.

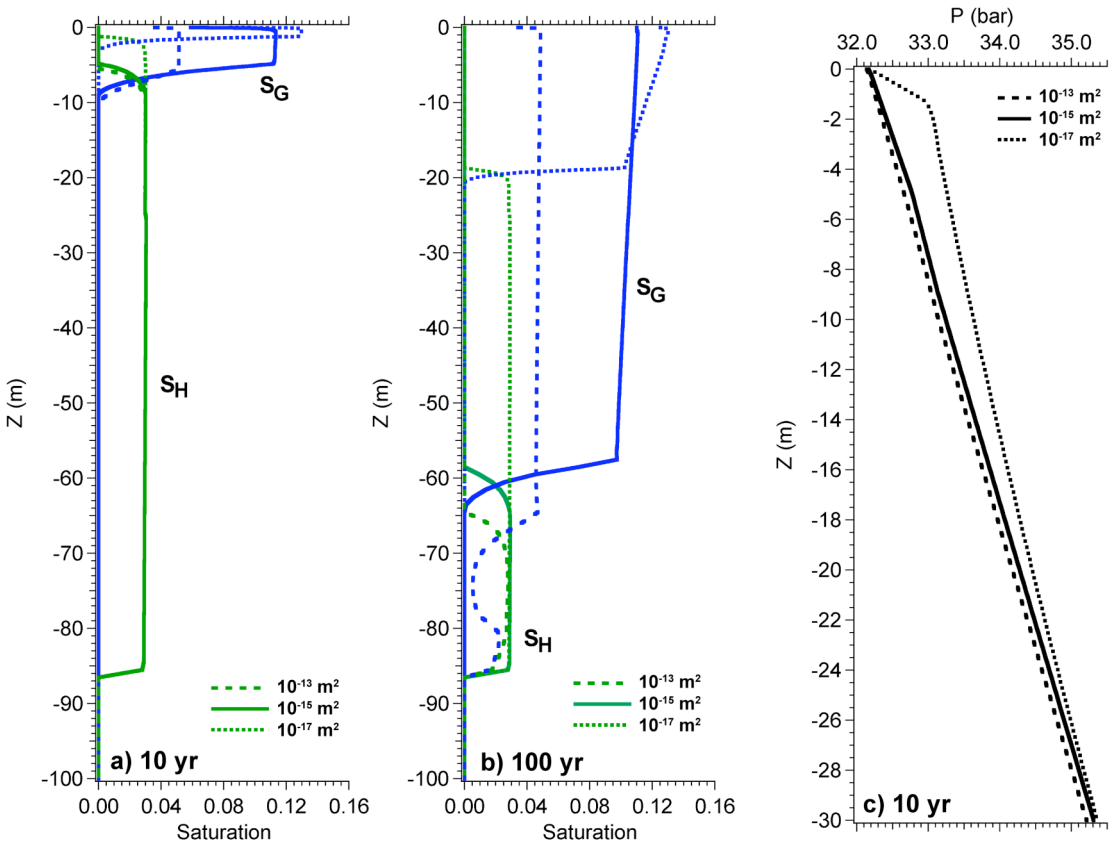

Figure 10: Profiles of S_H and S_G at t = 10 yr and t = 100 yr, plus the P profiles at t = 10 yr, for systems with permeabilities $k = 10^{-13}$, 10^{-15}, and 10^{-17} m^2, for Case II undergoing a 3 ^{o}C increase over 100 yr.

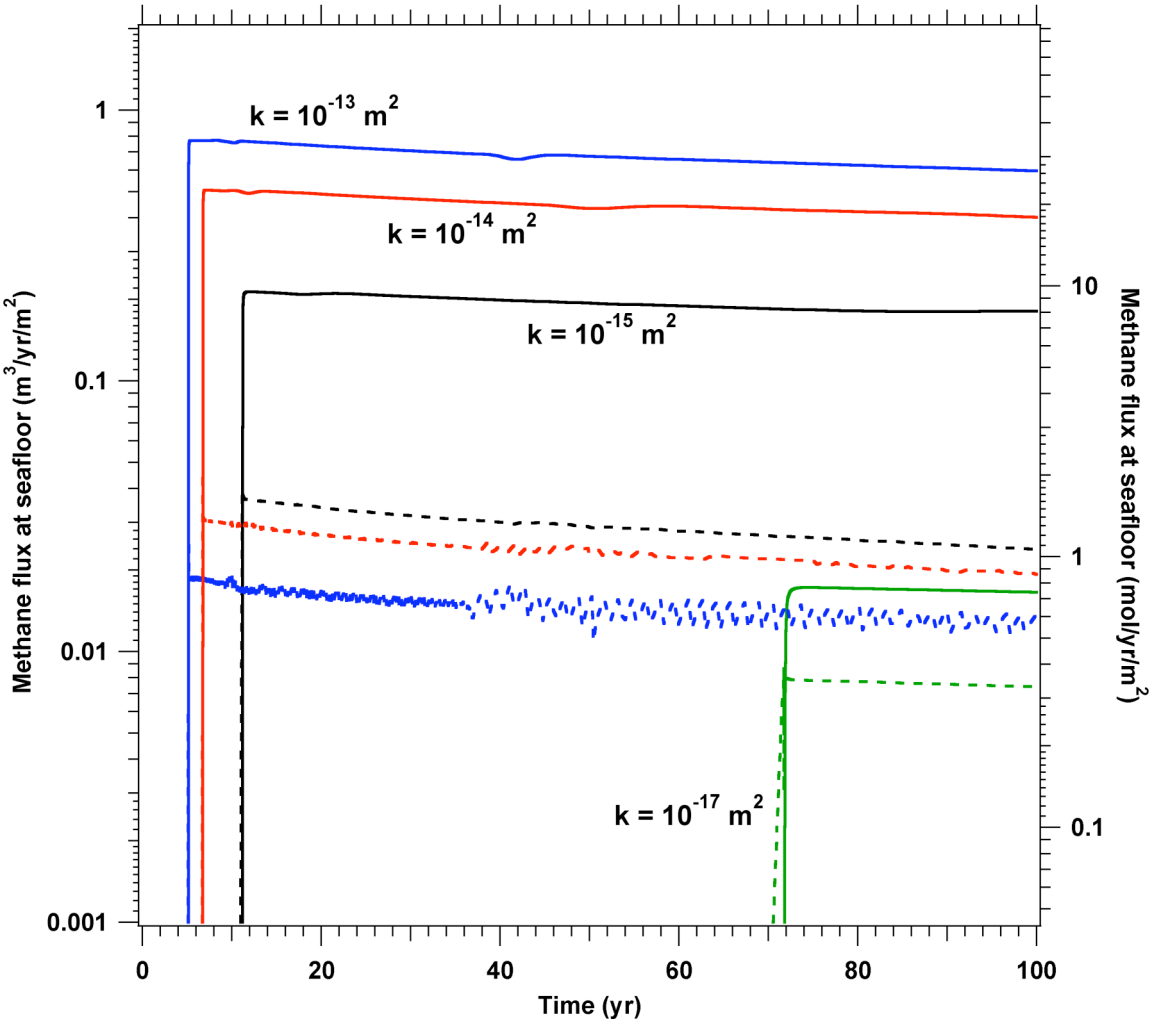

Figure 11: Variation of methane flux with sediment permeability, for Case III undergoing a 3 ^{o}C increase over 100 yr. Aqueous methane fluxes are represented by dotted lines, gas fluxes by solid lines.

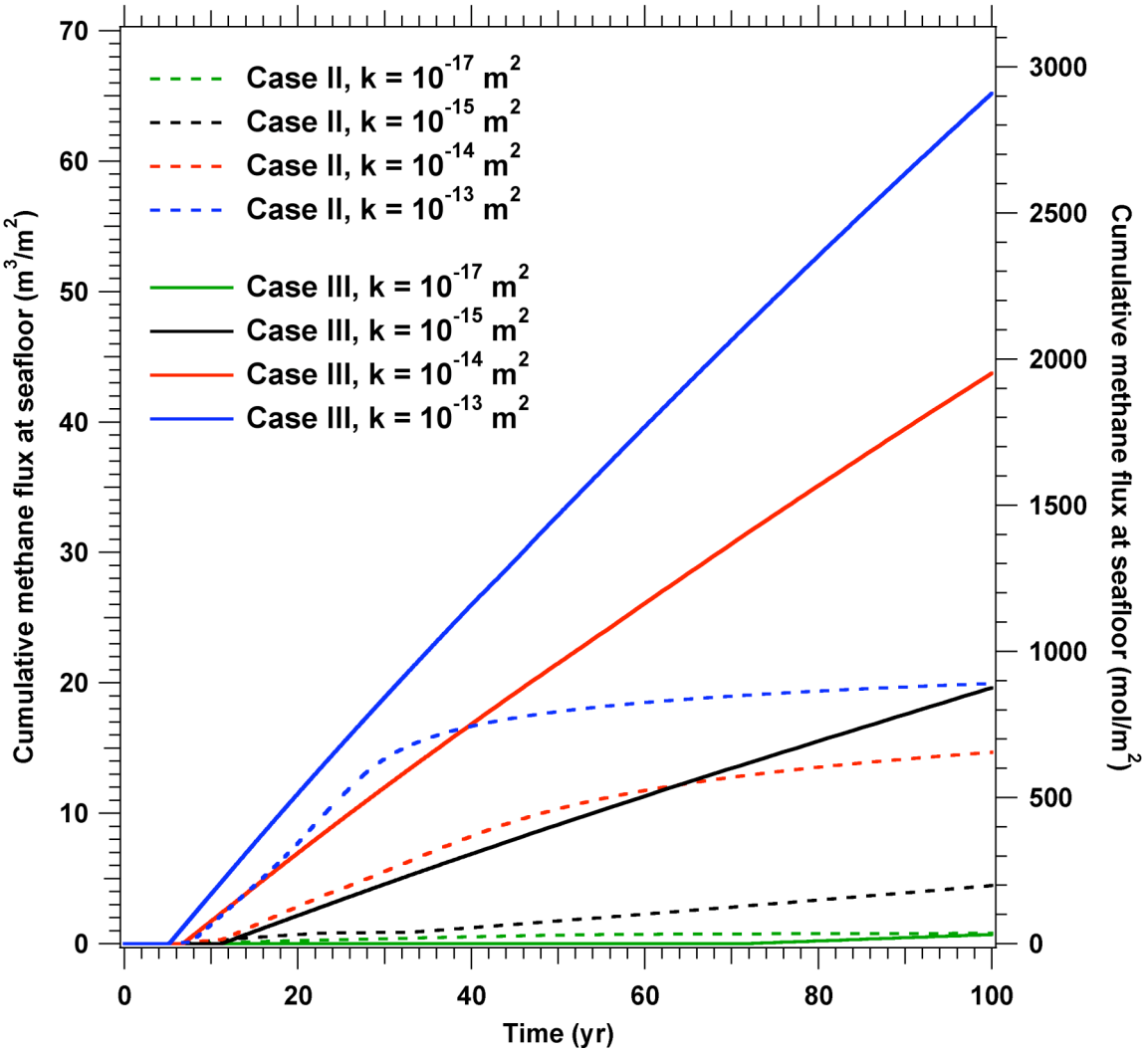

Figure 12: Cumulative methane release vs. depth and sediment permeability, for Case II and Case III systems undergoing a 3 ^{o}C increase over 100 yr.

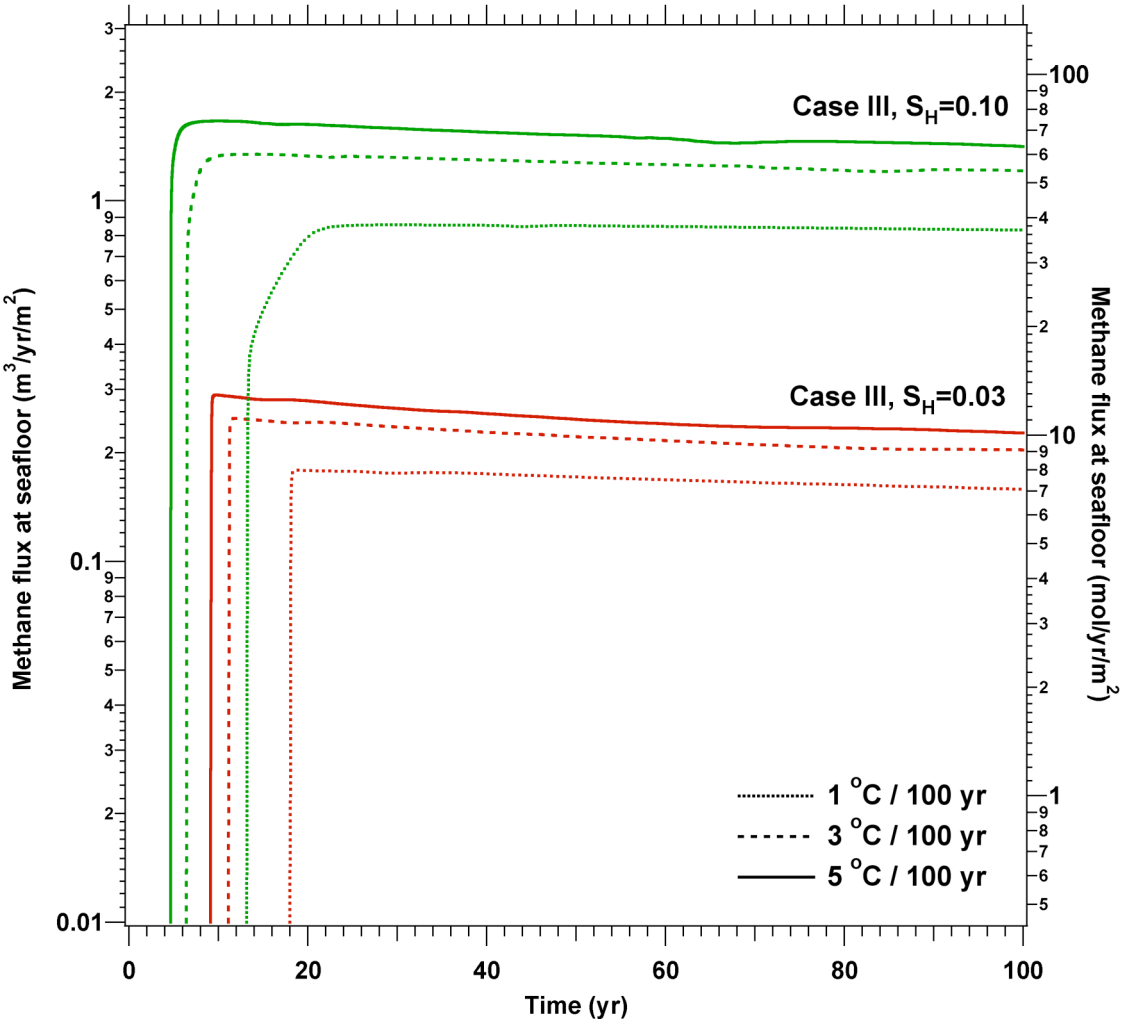

Figure 13: Variation of methane flux with initial hydrate saturation for Case III undergoing a 3°C increase over 100 years.

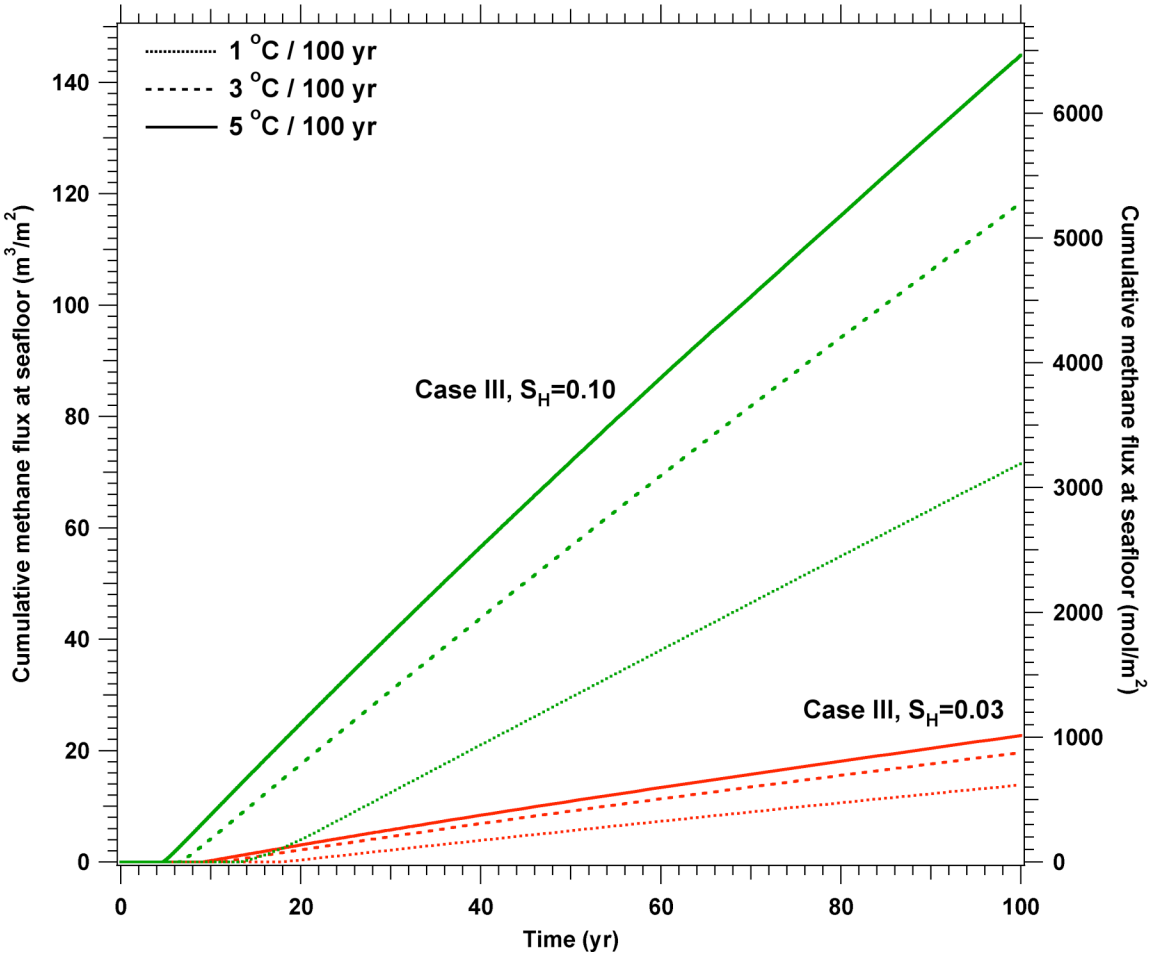

Figure 14: Cumulative methane release vs. initial hydrate saturation for Case III systems undergoing 1, 3, and 5 °C increases over 100 years.

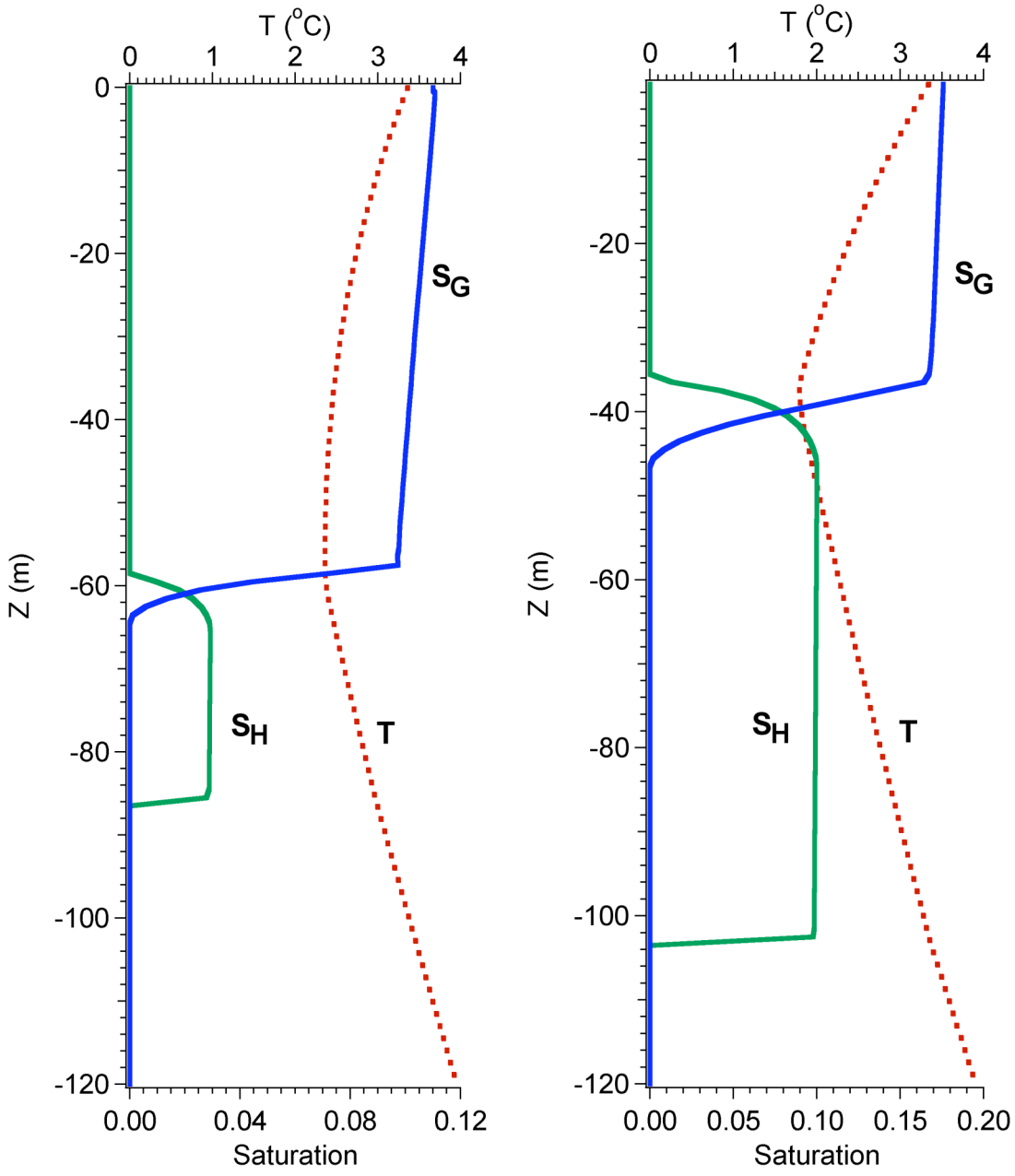

Figure 15: Profiles of hydrate and gas saturation, with temperature, for Case III at S_H = 0.03 and an elevated initial saturation of S_H = 0.10, after undergoing a 3°C increase over 100yr.

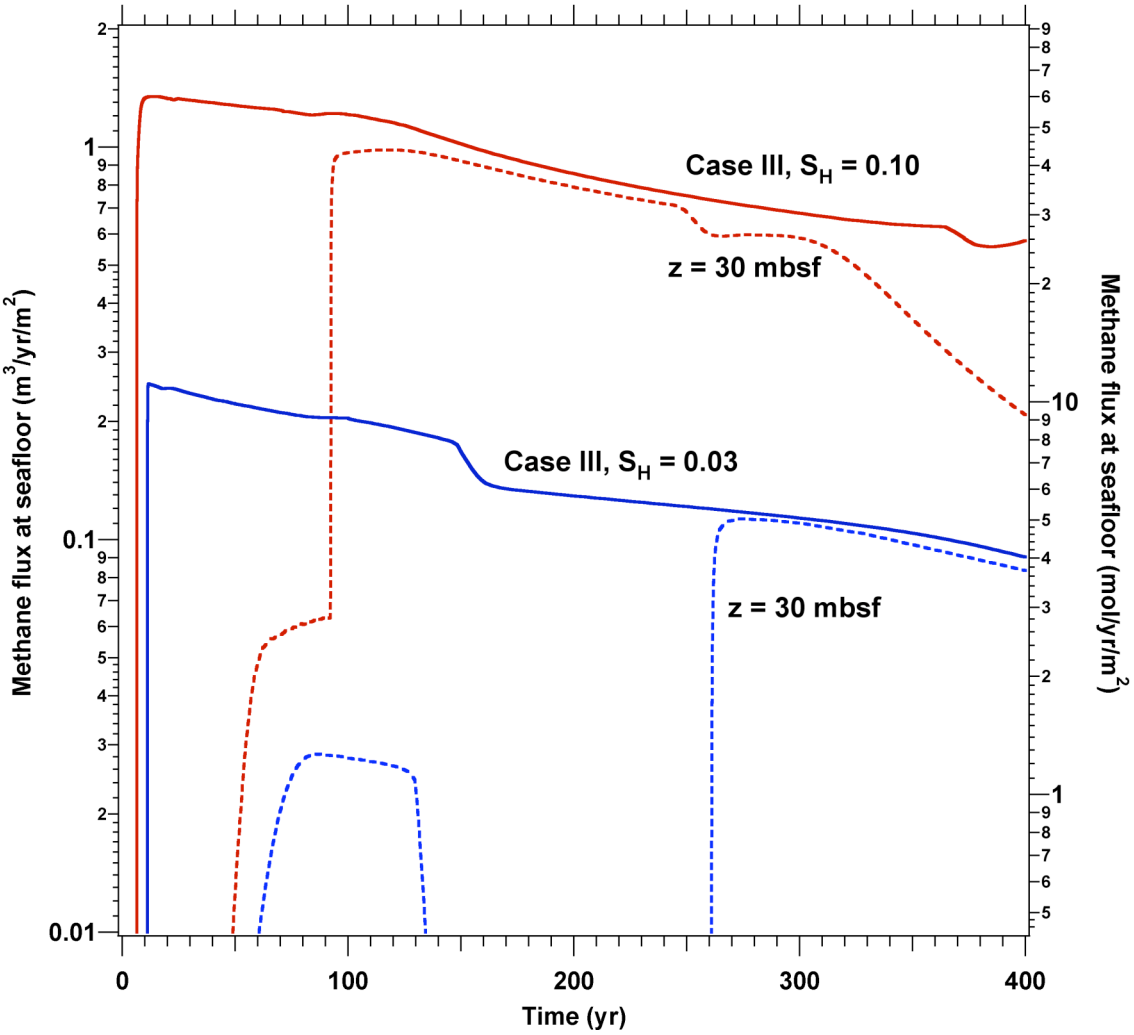

Figure 16: Variation of methane flux with depth of the top of the hydrate deposit for Case III, with $S_H = 0.03$ and $S_H = 0.10$, undergoing a 3°C increase over 100 years.

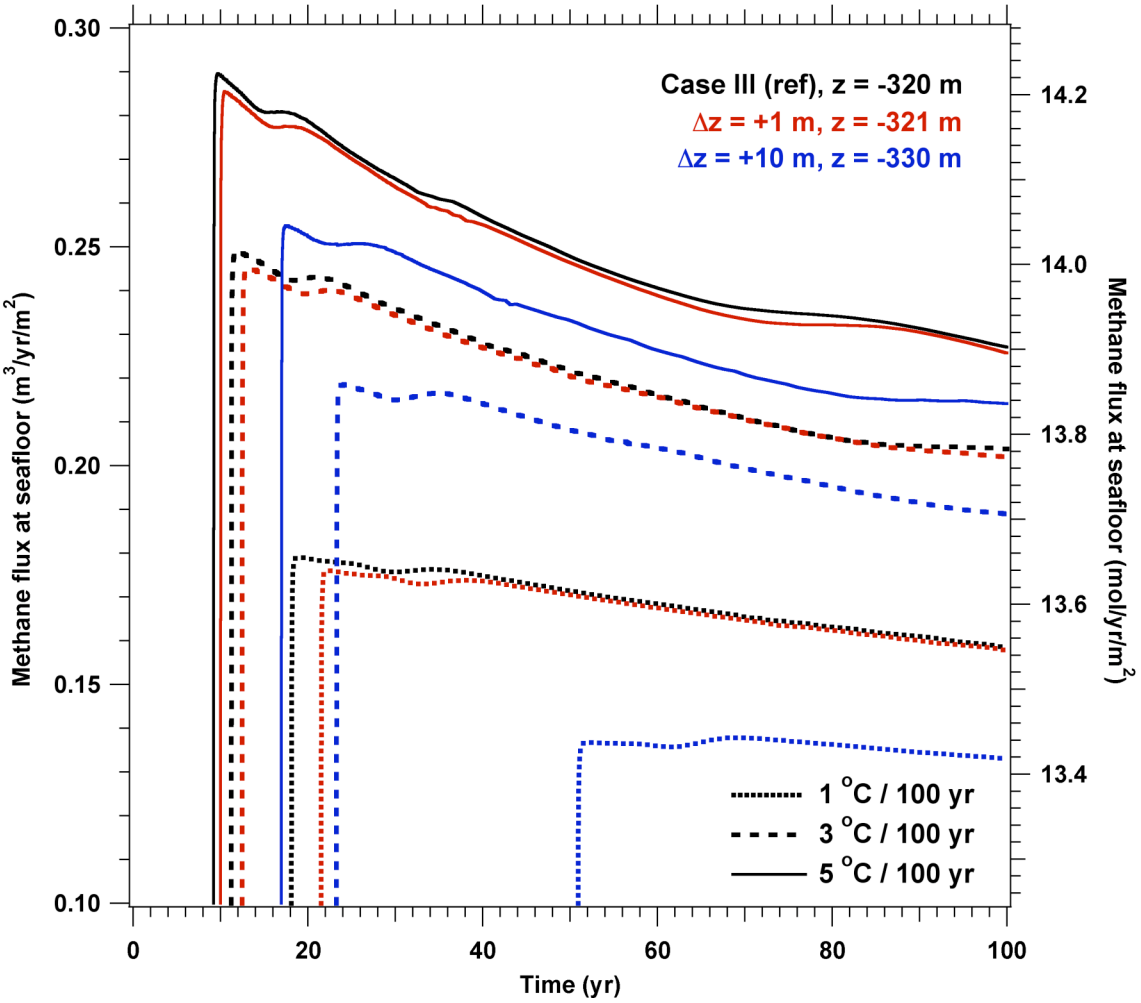

Figure 17: Variation of methane flux with sea level (depth of the overlying ocean) for Case III (S_H = 0.03) undergoing 1, 3, and 5 °C increases over 100 years.